Bioactive Materials 48 (2025) 564–582

Contents lists available at ScienceDirect

Bioactive Materials

journal homepage: www.keaipublishing.com/en/journals/bioactive-materials

Single-cell RNA sequencing-guided engineering of mitochondrial therapies for intervertebral disc degeneration by regulating mtDNA/SPARC-STING signaling

Guoyu Yang [a,b], Chenpeng Dong [a], Zhaoxi Wu [c], Peng Wu [d], Cao Yang [a], Lanlan Li [e,*], Jianxiang Zhang [b,f,g,**], Xinghuo Wu [a,***]

[a] Department of Orthopaedics, Union Hospital, Tongji Medical College, Huazhong University of Science and Technology, Wuhan, 430022, China
[b] Department of Pharmaceutics, College of Pharmacy, Third Military Medical University (Army Medical University), Chongqing, 400038, China
[c] School of Basic Medicine, Tongji Medical College, Huazhong University of Science and Technology, Wuhan, 430022, China
[d] College of Pharmacy and Medical Technology, Vocational and Technical College, Hanzhong, Shaanxi, 723000, China
[e] Department of Pharmaceutical Analysis, College of Pharmacy, Third Military Medical University (Army Medical University), Chongqing, 400038, China
[f] Yu-Yue Pathology Scientific Research Center, 313 Gaoteng Avenue, Jiulongpo District, Chongqing, 400039, China
[g] State Key Laboratory of Trauma and Chemical Poisoning, Third Military Medical University (Army Medical University), Chongqing, 400038, China

ARTICLE INFO

Keywords:
Intervertebral disc degeneration
Inflammation
Engineered mitochondria
Biotherapy
STING signaling

ABSTRACT

Intervertebral disc degeneration (IVDD) is a leading cause of discogenic low back pain, contributing significantly to global disability and economic burden. Current treatments provide only short-term pain relief without addressing the underlying pathogenesis. Herein we report engineering of biomimetic therapies for IVDD guided by single-cell RNA-sequencing data from human nucleus pulposus tissues, along with validation using animal models. In-depth analyses revealed the critical role of mitochondrial dysfunction in fibrotic phenotype polarization of nucleus pulposus cells (NPCs) during IVDD progression. Consequently, mitochondrial transplantation was proposed as a novel therapeutic strategy. Transplanted exogeneous mitochondria improved mitochondrial quality control in NPCs under pathological conditions, following endocytosis, separate distribution or fusion with endogenous mitochondria, and transfer to neighboring cells by tunneling nanotubes. Correspondingly, intradiscal mitochondrial transplantation significantly delayed puncture-induced IVDD progression in rats, demonstrating efficacy in maintaining mitochondrial homeostasis and alleviating pathological abnormalities. Furthermore, exogenous mitochondria were engineered with a bioactive, mitochondrial-targeting macromolecule to impart anti-oxidative and anti-inflammatory activities. The obtained multi-bioactive biotherapy exhibited significantly enhanced benefits in IVDD treatment, in terms of reversing IVDD progression and restoring structural integrity through the mtDNA/SPARC-STING signaling pathways. Overall, our engineered mitochondrial therapies hold great promise for treating IVDD and other musculoskeletal diseases linked to mitochondrial dysfunction.

1. Introduction

The intervertebral disc (IVD) comprises a central gelatinous nucleus pulposus (NP) encircled by a dense annulus fibrosus (AF), with both structures sandwiched between cartilaginous endplates. The progressive aging of the global population has led to a significant increase in the

Peer review under the responsibility of KeAi Communications Co., Ltd.

* Corresponding author. Department of Pharmaceutical Analysis, College of Pharmacy, Third Military Medical University (Army Medical University), 30 Gaotanyan Main Street, Chongqing 400038, China.

** Corresponding author. Department of Pharmaceutics, College of Pharmacy, Third Military Medical University (Army Medical University), 30 Gaotanyan Main Street, Chongqing, 400038, China.

*** Corresponding author. Department of Orthopedics, Union Hospital, Tongji Medical College, Huazhong University of Science and Technology, No.13 Hangkong Road, Wuhan 430022, Hubei Province, China.

E-mail addresses: lllan07@tmmu.edu.cn (L. Li), jxzhang1980@gmail.com, jxzhang@tmmu.edu.cn (J. Zhang), wuxinghuo@hust.edu.cn (X. Wu).

https://doi.org/10.1016/j.bioactmat.2025.02.036
Received 29 October 2024; Received in revised form 13 February 2025; Accepted 23 February 2025

prevalence of IVDD, a pathological condition that frequently manifests as discogenic low back pain, spinal stenosis, and intervertebral disc herniation [1,2]. Notably, low back pain is a major public health challenge that affects approximately 80 % of the worldwide population during their lifetime, thus resulting in profound disability burdens and imposing substantial socioeconomic impacts [3]. IVDD is pathologically characterized by progressive depletion of proteoglycans, disorganization of extracellular matrix (ECM) components, and remarkable reduction in disc height. The precise pathophysiological mechanisms underlying IVDD progression remain incompletely understood. Current research, however, has identified multiple etiological factors, including mechanical trauma, age-related degeneration, nutritional deficits, inflammatory cascades, biochemical stressors, and various noxious stimuli. The disease pathogenesis involves a complex and multifactorial interplay of diverse cellular and molecular pathways, encompassing biomechanical alterations in spinal structures, progressive ECM degradation, sustained low-grade inflammatory responses, oxidative damage, fibrotic changes, impaired autophagic processes, and cell loss due to senescence, apoptosis, and pyroptosis [4,5].

In clinical practice, symptomatic IVDD is typically treated through pharmacological therapies, rehabilitation, and surgical interventions. In particular, pharmacological intervention is often employed for the conservative management of discogenic low back pain. Conventional pharmacotherapies for IVDD, such as steroids, non-steroidal anti-inflammatory drugs, analgesics, and muscle relaxants, alleviate pain symptoms primarily through reducing inflammatory components in the pain pathways or tackling both inflammation and pain [6]. However, current pharmacological approaches predominantly target neuropathic and radicular pain symptom management, failing to address the fundamental pathological processes, reverse disc degeneration, restore native tissue structure, or reconstruct the spinal biomechanical function. Consequently, these treatment options provide only short-term relief, with patients often experiencing frequent recurrences of symptoms and gradual aggravation of IVDD. Recently, recognizing the pivotal roles of inflammation, immunometabolic alternations, tissue and cell homeostasis, and associated signaling pathways in the onset and progression of IVDD [2,4,5,7], various new therapies have been investigated in animal models and clinical trials. These include tumor necrosis factor (TNF)-α antibodies, interleukin (IL)-1 receptor antagonists, anti-IL-6 receptor therapies, enzyme inhibitors, transforming growth factor (TGF)-β superfamily agents, anabolic and anti-catabolic compounds, and specific nucleic acid therapies [8]. Beyond these molecular therapies, emerging strategies utilizing chondrocytes, IVD cells, stem cells, and cell-derived extracellular vesicles have shown promising therapeutic potential for IVD regeneration [9–11]. These innovative approaches have demonstrated multifaceted benefits, including attenuation of chronic inflammation, inhibition of cellular senescence and programmed cell death of NP cells (NPCs), normalization of metabolic homeostasis, restoration of disc morphology and structural integrity, and preservation of spinal biomechanical function.

Recently, advanced delivery systems have been rationally designed and developed, to address the inherent limitations of molecular therapies, such as rapid systemic distribution, short local retention time, enzymatic hydrolysis, and therapeutic inactivation in the harsh and complex microenvironment of degenerated discs. These include nanocarriers, microspheres, macroscale vehicles, and multiscale or composite delivery systems, all engineered to achieve precise spatiotemporal control and sustained therapeutic release within the target tissue [12–17]. Meanwhile, functionalized hydrogels, biomimetic scaffolds, and electrospun nanofibers have been explored to enhance survival, promote proliferation, and facilitate differentiation of therapeutic cells (such as NPCs and stem cells) within degenerated discs [18–22]. These biomaterial-based systems have also been examined for phenotypic modulation of NPCs, in situ NP replacement, AF repair, and holistic IVD regeneration [21,23–25]. Such multifunctional drug delivery and tissue engineering strategies exhibit promising potential for decelerating degenerative cascades and promoting functional tissue repair [21]. Despite these advancements, therapeutic advantages of these approaches remain controversial. In particular, neither the advanced drug delivery systems, biomaterial strategies, nor tissue engineering approaches have successfully progressed to clinical trials. This underscores the crucial need for innovative therapeutic paradigms to overcome the multifaceted challenges of IVDD treatment.

Accumulating evidence has demonstrated that mitochondrial dysfunction plays a central role in the pathogenesis of IVDD. Mitochondria have been recognized not only as key regulators of energy metabolism in NPCs, but also as contributors to oxidative stress, inflammation, and the fibrotic process when their function is disrupted [26–28]. However, therapeutic effects of exogenous mitochondrial transplantation in IVDD treatment remain to be fully elucidated. Herein we propose the development of mitochondrial therapies for IVDD guided by single-cell RNA-sequencing (scRNA-seq) analysis. First, in-depth analyses of scRNA-seq data from human NP tissues with varied severities of IVDD, followed by validation with animal models, revealed the critical role of mitochondrial dysfunction in mediating fibrotic phenotype polarization of NPCs during the progression of IVDD. We then demonstrated the effectiveness of mitochondrial transplantation in NPCs and a rat model of IVDD, mechanistically via modulating mitochondrial quality control. Furthermore, considering the contribution of oxidative stress and inflammation to IVDD progression, we designed and synthesized a bioactive, mitochondrial-targeting macromolecule for mitochondrial engineering (Fig. 1A–B). This functionalized multi-bioactive mitochondrial therapy exhibited significantly enhanced efficacy in alleviating IVDD, mainly by regulating the mtDNA/SPARC-STING axis (Fig. 1C–E).

2. Results

2.1. scRNA-seq analysis indicates the pivotal role of mitochondrial malfunction in the fibrotic phenotype polarization of NPCs in disc degeneration

Whereas previous studies showed that mitochondrial dysfunction plays a critical role in the pathogenesis of IVDD [5,7], its exact effects on specific cell types in degenerated discs remain to be addressed. To uncover the states of mitochondrial pathophysiology in NPCs during IVDD, we re-analyzed single-cell transcriptome data of human NP tissues from 7 individuals with various Pfirrmann grading scores from GEO database based on our previous study [29]. Few immune cells were identified in healthy tissues (Pfirrmann I), consistent with existing findings that classify the IVD as an immune-privileged tissue [30]. By contrast, their infiltration was notably increased in degenerative NP tissues (Pfirrmann II-V) (Figs. S1A–B). Then NPCs expressing sex-determining region Y-box 9 (SOX9), aggrecan (ACAN), or collagen type II alpha 1 chain (COL2A1) were separated for further unsupervised cell clustering and 7 distinctive subgroups were annotated based on their highly expressed genes, including adhesion NPCs, fibrochondrocytes, effector NPCs, regulatory NPCs, HT-CLNPs, proliferative NPCs, and homeostatic NPCs (Fig. 2A–B). The component of NPC subpopulations showed notable differences between healthy and degenerative NP tissues (Fig. 2C). Specifically, homeostatic NPCs were decreased in degenerative NP tissues, which were nearly undetectable in NP tissues classified as Pfirrmann grade V. By contrast, the subpopulations of fibrochondrocytes and adhesion NPCs demonstrated substantial expansion. Notably, both cell subtypes exhibited elevated expression profiles of genes associated with fibrosis, a common pathological process of IVDD. Moreover, tissue preference was analyzed in subpopulations of homeostatic NPCs and fibrochondrocytes within a comprehensive dataset encompassing 36,213 NPCs. This dataset comprised 3 healthy NP tissue samples (Pfirrmann I), 4 mildly degenerated samples (Pfirrmann II-III), and 4 severely degenerated samples (Pfirrmann IV-V) (Figs. S1C–F). These results collectively suggest that fibrotic polarization of NPCs plays an important role in NP

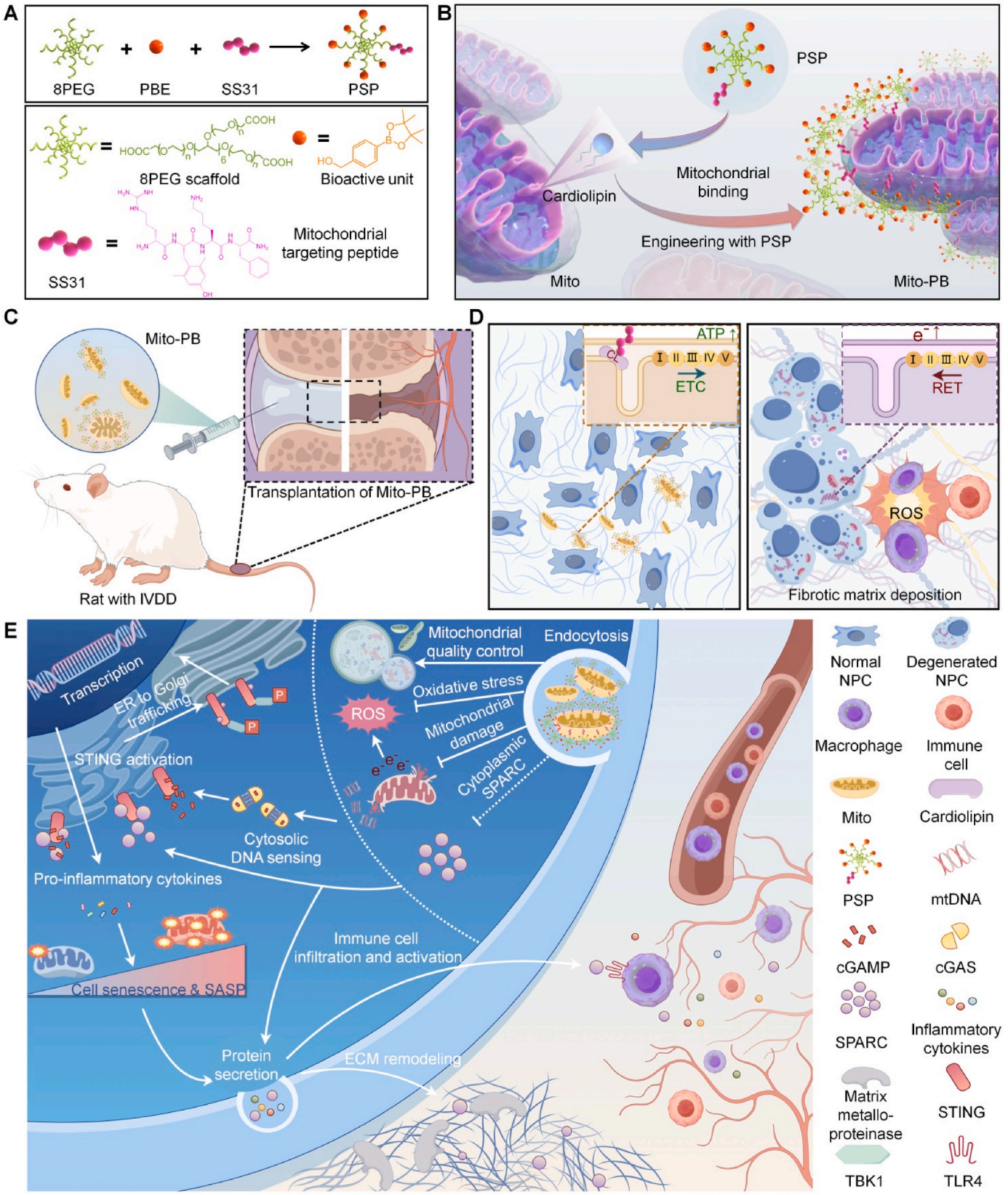

(caption on next page)

Fig. 1. Schematic illustration of engineering of functionalized mitochondria for effective treatment of IVDD. (A) A sketch showing the rational design and development of an anti-oxidative, anti-inflammatory, and mitochondrial-targeting PSP, which was synthesized by sequentially conjugating seven bioactive PBE units and one mitochondrial-targeting peptide SS31 onto each 8-arm polyethylene glycol chain. (B) Schematic illustration of mitochondrial engineering using PSP via specific binding to cardiolipin. (C) Intradiscal transplantation of the engineered mitochondria restores a normal gelatinous matrix of the NP tissue in rats with IVDD. (D) Distinctive pathophysiological microenvironments in the revitalized and degenerated disc tissues. The left panel shows that NPCs with normal structure are organized uniformly in the ECM after treatment with engineered mitochondria, by improving the mitochondrial respiratory chain. The right panel illustrates that mitochondria with declined MMP accumulate in degenerated NPCs, thus leading to a shift from ATP production to massive superoxide anion leakage through RET and exacerbated oxidative stress, concomitant with abnormal fibrosis. (E) Cellular and molecular mechanisms underlying therapeutic effects of transplanted functional mitochondria. The engineered multifunctional mitochondria can promote mitochondrial quality control, attenuate oxidative and pro-inflammatory responses, inhibit mtDNA leakage, and reduce cytosolic SPARC production, thus suppressing the STING signaling activity triggered by cytosolic mtDNA and SPARC. Subsequently, ECM remodeling is improved, and fewer immune cells infiltrate the disc tissue due to decreased secretion of pro-inflammatory cytokines and fibrotic proteins from NPCs. Images were created with Figdraw.com.

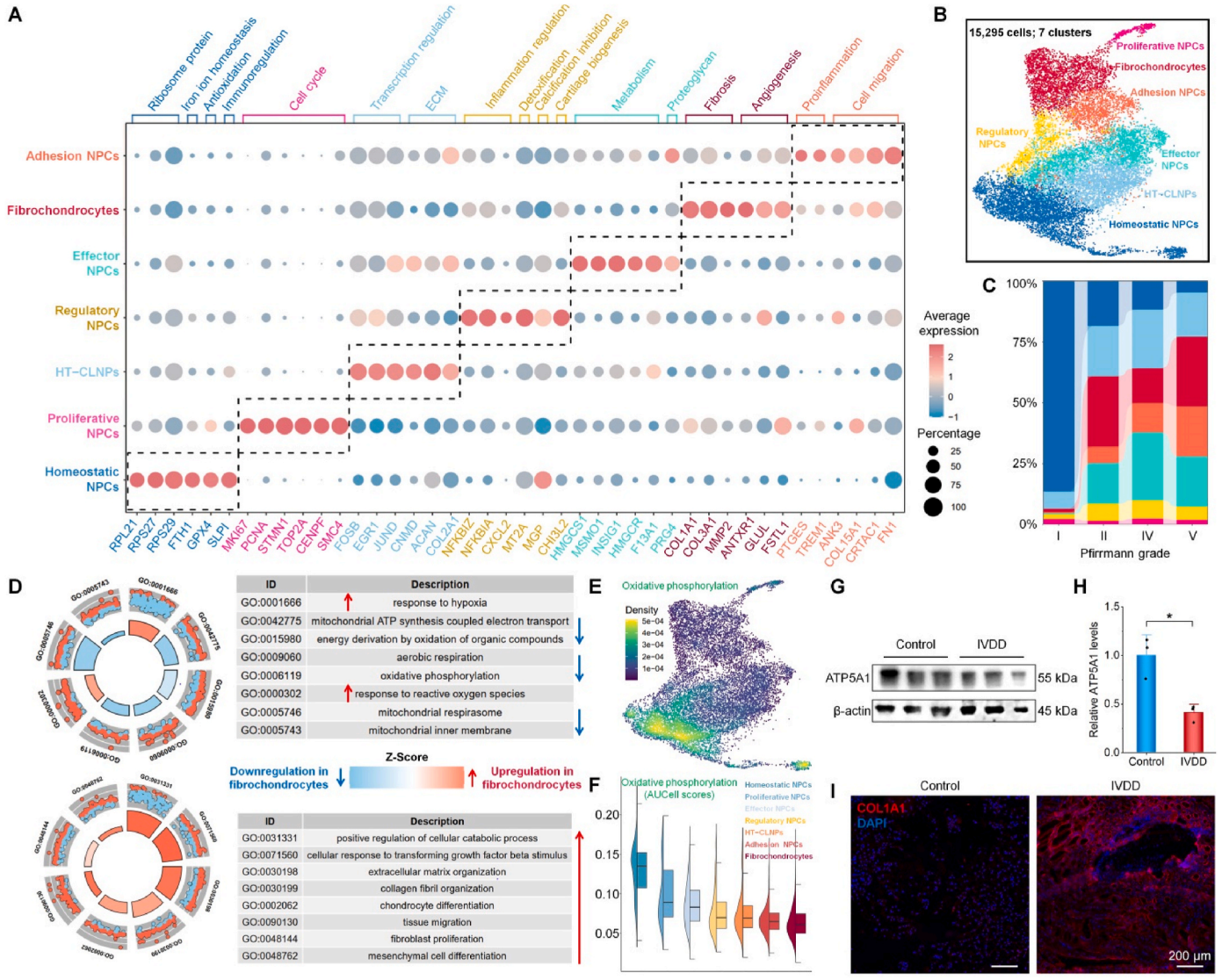

Fig. 2. Analysis of scRNA-seq data indicates mitochondrial malfunction in the degenerated NPC cluster that is characterized by a fibrotic phenotype. (A) The heatmap of marker genes of distinctive subclusters in the scRNA-seq data from 7 human NP tissues. (B) The UMAP plot of the scRNA-seq data, including 15,295 cells of 7 cell subtypes from human NP tissues. (C) Proportions of different subsets of NPCs. (D) GO enrichment analyses of DEGs among fibrochondrocytes and homeostatic NPCs as well as Z-scores of each GO term. The colors of the inner circles in the left panel indicate the regulation direction of enriched GO terms. (E–F) The UMAP image (E) and violin plot (F) show oxidative phosphorylation activity in NPCs in the scRNA-seq data, as defined using the AUCell algorithm. (G–H) Typical Western blot bands (G) and quantitative analysis (H) of ATP5A1 protein levels in the normal and degenerated rat disc tissues. (I) Immunofluorescence analysis of COL1A1 in the normal and degenerated rat discs. Data in (H) are presented as means ± SD (n = 3). Statistical differences were analyzed using the unpaired student's test with a two-tailed distribution. *P < 0.05.

tissue degeneration, in line with previous findings [1,31].

We further assessed the differentially expressed genes (DEGs) among fibrochondrocytes and homeostatic NPCs by gene ontology (GO) analysis. Besides, Z-scores of GO terms were calculated to indicate their regulation directions. It was found that genes responsible for oxidative phosphorylation (OXPHOS) and the components of mitochondrial

respirasome were significantly downregulated in fibrochondrocytes. Comparatively, DEGs involved in fibrosis and the ECM catabolic processes were upregulated in fibrochondrocytes (Fig. 2D). Gene set scoring via AUCell also revealed the OXPHOS disorder, as implicated by the signal intensities of uniform manifold approximation and projection (UMAP) plots (Fig. 2E–F). Moreover, Western blot analysis and immunofluorescence staining indicated that collagen type I alpha 1 chain (COL1A1), a key component of fibrotic tissues, was enriched in degenerated rat discs but not in healthy discs. By contrast, the protein level of ATP synthase subunit alpha (ATP5A1), one of the mitochondrial complex V subunits, was reduced substantially in the degenerated IVD, compared to that in normal discs (Fig. 2G–I). Taken together, these results indicate that increased fibrotic polarization of NPCs is associated with impaired OXPHOS activity. This suggests an intimate relationship between fibrosis and mitochondrial malfunction in the progression of IVDD. Therefore, effective regulation of mitochondrial activity represents a promising strategy for the treatment of IVDD by inhibiting fibrosis and restoring the normal gelatinous matrix of NPCs.

2.2. Characterization of mitochondria isolated from rat cardiomyocytes and their cellular uptake profiles

Given our scRNA-seq analysis highlighted the pivotal role of mitochondrial dysfunction in the pathogenesis of IVDD, we hypothesize that exogenous mitochondrial supplementation in the degenerated NP tissue can serve as a promising novel strategy for IVDD treatment. As a proof-of-concept study, mitochondria were initially isolated from the healthy rat myocardial tissues, capitalizing on the enrichment of mitochondria in cardiomyocytes. Furthermore, there are well-established, reliable protocols for isolating mitochondria from the cardiac tissue [32]. Observation by transmission electron microscopy (TEM) revealed intact and spherical structure for the purified myocardial mitochondria (termed as Mito), clearly showing smooth outer membrane, highly folded inner membrane (i.e., cristae), and intermembrane space between the outer and inner membranes (Fig. 3A). The obtained Mito was further confirmed by fluorescence microscopy after staining with a specific probe Mito-Tracker Green (MTG) (Fig. 3B). Quantification by dynamic light scattering (DLS) indicated that the average diameter of Mito was 611 nm (Fig. 3C), with ζ-potential of -7.8 ± 0.5 mV (Fig. S2). These results demonstrated the successful preparation of Mito.

Mito is anticipated to exert its therapeutic effects in NPCs, with efficient cellular uptake being a crucial prerequisite. Therefore, we examined cellular internalization profiles of MTG-labeled Mito in rat NPCs (Fig. 3D). Confocal microscopic observation and flow cytometric quantification showed time-dependent cellular internalization of Mito in NPCs (Fig. 3E–G). Endocytosis is a common mechanism responsible for the internalization of exogenous particles. The endocytic pathway, while facilitating mitochondrial uptake, presents a critical biological barrier due to lysosomal degradation. Successful endolysosomal escape is crucial for preserving mitochondrial integrity, as prolonged lysosomal entrapment can lead to complete proteolytic degradation and consequent loss of mitochondrial bioactivity. By contrast, following lysosomal escape, exogenous mitochondria can persist in the cytoplasm, thereby maintaining ATP synthesis capacity and participating in cellular metabolism. Besides, the functional mitochondria can be integrated into the endogenous mitochondrial network through fusion processes, enabling metabolic complementation in recipient cells. Consequently, we investigated the lysosomal escape of internalized Mito. Within 2 h of mitochondrial transplantation, almost all internalized Mito (green fluorescence) overlapped with LysoTracker Red-labeled lysosomes (red fluorescence), resulting in yellow signals (Fig. 3H). At 4 and 8 h post-transplantation, separate green signals were clearly observed within NPCs, indicating successful lysosomal escape. This result based on NPCs agrees with the previous studies in cardiomyoblasts and endothelial cells that exogenous mitochondria were internalized via macropinocytosis [32,33], a form of endocytosis mediated by large vesicles resulting from membrane ruffling and extension. Furthermore, confocal microscopy with Z-stack scanning revealed the intracellular distribution of either separate MTG-labeled Mito or Mito co-localizing with endogenous mitochondria labeled with Mito-Tracker Deep Red (MTDR) (Fig. 3I).

Meanwhile, intercellular mitochondrial transfer has been observed between different cell types, such as from stem cells to alveolar cells [34,35], endothelial cells [33], and T cells [36], as well as from astocytes to neurons [37,38]. Mitochondrial transfer from hematopoietic cells to immune, epithelial, endothelial, and stromal cells was also reported most recently [39]. This transfer can be achieved through different ways, including tunneling nanotubes (TNTs), extracellular vesicles, and gap junction channels [40]. In particular, TNTs-mediated transfer has been considered as the dominating approach [41]. In NPCs, we found the presence of exogenously supplemented MTG-labeled Mito in TNTs (Fig. 3J), suggesting that transplanted Mito can also achieve intercellular trafficking through this nanotubular pathway. Notably, TNTs are specialized intercellular communication channels that can facilitate the transport of various cellular components between connected cells [42]. The formation of TNTs involves the reorganization of cytoskeletal components. The transport of mitochondria through TNTs is likely an active process that requires the dynamic involvement of motor proteins such as myosin and dynamin, which are essential for mitochondrial trafficking [40]. The transport and exchange of endogenous mitochondria via TNTs are considered crucial for cellular stress responses, damage repair, and intercellular energy homeostasis [42].

Collectively, high-purity Mito was successfully isolated from the rat cardiac tissue. Mito can be efficiently internalized into NPCs by endocytic/macropinocytic pathways. Following internalization, the exogenous Mito not only distributed freely within the cytoplasm but also underwent fusion with endogenous mitochondrial networks in recipient NPCs. Moreover, the internalized Mito in NPCs can be transported to adjacent NPCs through intercellular transfer via TNTs (Fig. 3K).

2.3. Mito transplantation revitalizes mitochondria in NPCs by activating mitochondrial quality control

As well documented, mitochondrial dysfunction is generally accompanied with the abnormal structure, resulting from an imbalance in mitochondrial dynamics, such as excessive mitochondrial fission and fragmentation [43]. After challenging with ROS (Fig. 4A), confocal microscopic observation revealed notably short mitochondrial branches in NPCs, as compared to normal NPCs treated with fresh medium alone (Fig. 4B). By contrast, Mito supplementation remarkably normalized the mitochondrial branch length. Consistent results were found by TEM observation and subsequent quantitative analysis of mitochondrial area (Fig. 4C). Consequently, Mito transplantation can effectively improve the structure of damaged mitochondria in NPCs. Then we examined whether this strategy can restore impaired mitochondrial function of NPCs under pathological conditions. After 24 h of exposure to ROS, mitochondrial membrane depolarized in NPCs, as implicated by significantly reduced mitochondrial membrane potential (MMP) (Fig. 4D–E), a hallmark of mitochondrial malfunction. After intervention with Mito at concentrations ranging from 0.8×10^3, 4×10^3, to 20×10^3 per milliliter of culture medium, MMP of NPCs was significantly enhanced. It should be emphasized that these concentrations of Mito fall within the safe dose range, as confirmed by our cytotoxicity studies in NPCs (Fig. S3). In particular, ROS-stimulated NPCs treated with Mito at 20×10^3/mL exhibited MMP nearly comparable to normal NPCs (Fig. 4D–F). Consistently, Mito transplantation effectively reversed ATP production in ROS-induced NPCs, in a dose-dependent manner (Fig. 4G). Notably, the increased ATP production serves as an indicator of enhanced mitochondrial complex V activity [44].

In addition to their essential role as energy providers, mitochondria are the main source of ROS, primarily by regulating superoxide production at the electron transport chain (ETC). In response to harmful stimuli, leakage of superoxide produced by reverse electron transport

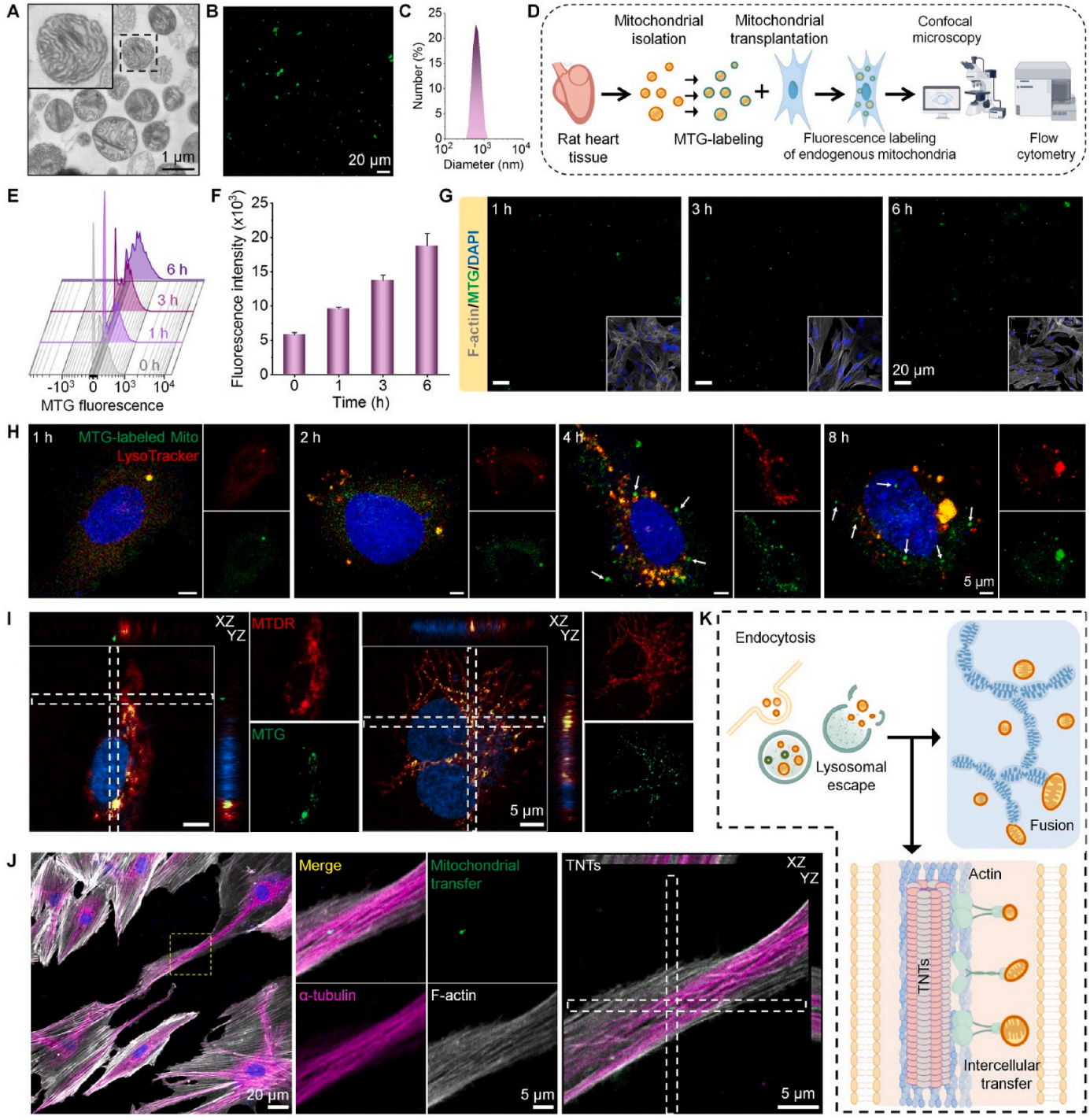

Fig. 3. Characterization of Mito as well as evaluation of cellular uptake, intracellular trafficking, and intercellular transfer profiles of Mito in NPCs. (A) A representative TEM image of Mito isolated from the rat cardiac tissue. (B) Fluorescence image of Mito labeled with MTG. (C) The size distribution of Mito. (D) A diagram showing the transplantation process for evaluating Mito cellular uptake profiles in NPCs. (E–F) Typical flow cytometric curves (E) and quantitative analysis (F) of time-dependent cellular uptake of MTG-labeled Mito in NPCs. (G) Fluorescence images showing time-dependent internalization of Mito in NPCs. (H) Fluorescence observation of intracellular trafficking of internalized Mito at 1, 2, 4, and 8 h post incubation. Endolysosomes were stained with Lysotracker (red), while Mito was labeled with MTG (green). (I) Z-stack scanning images indicate intracellular distribution profiles of transplanted Mito in NPCs. Endogenous mitochondria and Mito were stained with MTDR (red) and MTG (green), respectively. (J) Immunofluorescence images acquired via Z-stack scanning show intercellular transfer of transplanted Mito among NPCs through TNTs. α-Tubulin was labeled with Cy5 (pink), while F-actin and Mito were stained with Cy3 (grey) and MTG (green), respectively. (K) A sketch illustrates distribution and transfer of Mito after internalization in NPCs. Images in (D and K) were created with Figdraw.com. Data in (F) are presented as means ± SD (n = 3).

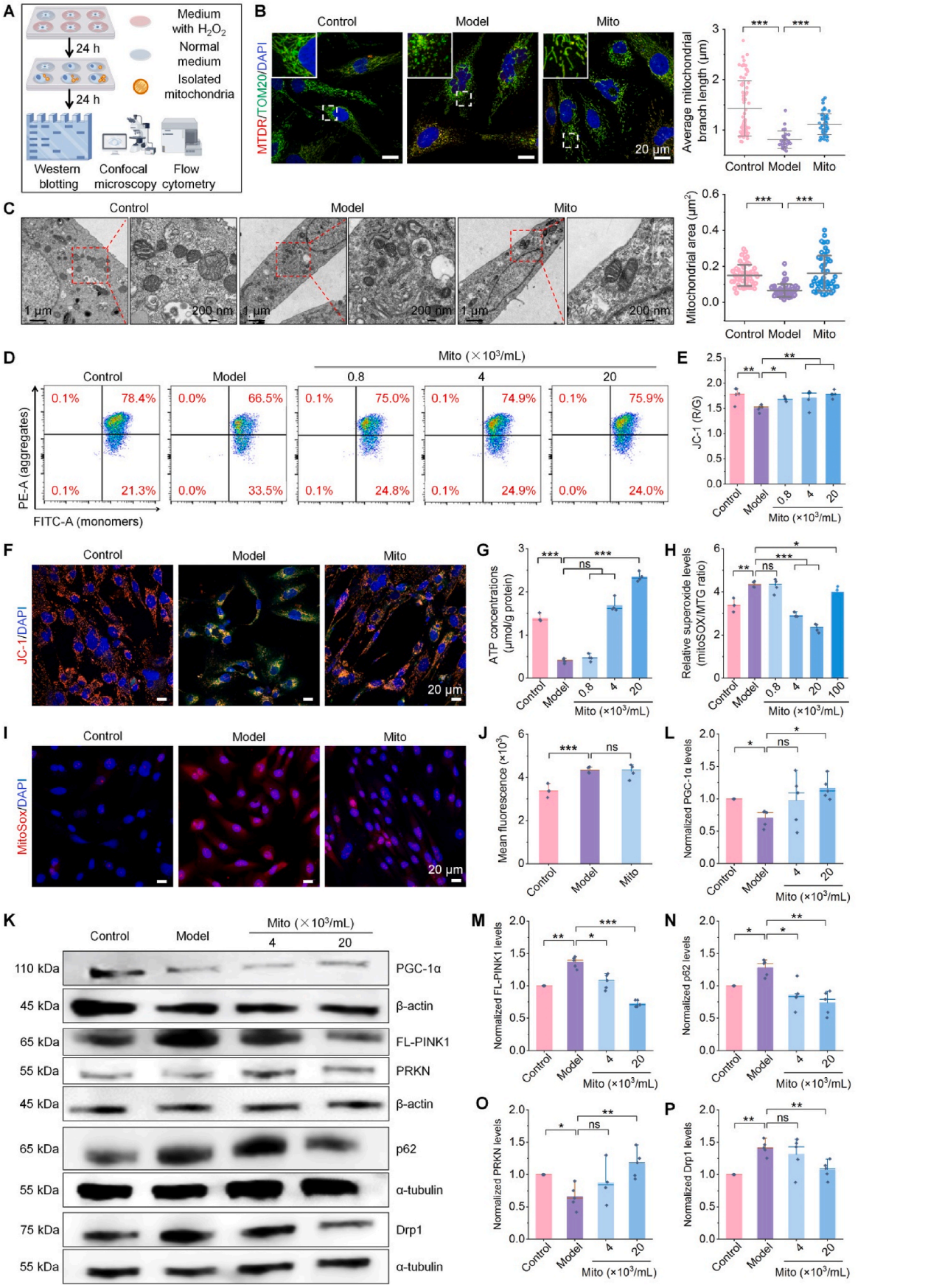

(caption on next page)

Fig. 4. Mito transplantation revitalizes mitochondria in ROS-stimulated NPCs by activating mitochondrial quality control. (A) A diagram shows treatment procedures for evaluating biological effects of Mito in NPCs. In the control group, NPCs were treated with fresh medium alone, while cells in the model group were induced with H_2O_2. For Mito groups, NPCs were stimulated with H_2O_2, followed by treatment with Mito at different doses. (B) Immunofluorescence images (left) and quantitative analysis (right) of mitochondrial length in NPCs after different treatments (Control, n = 71; Model, n = 27; Mito, n = 50). Endogenous mitochondria were stained with MTDR (red), while TOM20 was labeled by Alexa Fluor 488 (green). (C) Representative TEM images (left) and quantitative analysis of the average mitochondrial area (right) in NPCs after different treatments (Control, n = 51; Model, n = 57; Mito, n = 50). (D–E) Flow cytometric profiles (D) and quantitative analysis (E) of MMP of NPCs subjected to different treatments, as indicated by changes in red and green fluorescence intensity ratios (R/G) of a fluorescent probe JC-1 (n = 5). (F) Typical fluorescence images of NPCs stained with JC-1. Red, normal mitochondria; green, depolarized mitochondria; blue, nuclei stained with Hoechst. (G) Quantification of the cellular ATP content in NPCs (n = 4). (H) Flow cytometric analysis of mitochondrial superoxide production in NPCs after different treatments and staining with MitoSOX and MTG (n = 4). (I) Fluorescence images of NPCs stained with MitoSOX (red) and Hoechst (blue). (J) Flow cytometric quantification of total cellular ROS levels in NPCs post staining with DCFH-DA (n = 4). (K–P) Representative Western blot bands (K) and quantitative analysis of protein levels of PGC-1α (L), FL-PINK1 (M), p62 (N), PRKN (O), and Drp1 (P) in NPCs after different treatments (n = 5). Images in (A) were created with Figdraw.com. Data are presented as means ± SD. Statistical differences were determined using the one-way ANOVA with posthoc LSD or Tamhane's tests. *P < 0.05, **P < 0.01, and ***P < 0.001; ns, no significance.

(RET) from complex II to complex I exacerbates cellular stress, ultimately resulting in cell senescence and death [45]. Therefore, the antioxidant systems within mitochondria, including mitochondrial antioxidants (such as superoxide dismutase, cytochrome C, and glutathione), membrane proteins, and other regulatory mechanisms, are essential for maintaining cellular homeostasis. To examine whether transplanted Mito can eliminate ROS and modulate inflammation in cellular models, we detected both mitochondrial ROS and cellular ROS in NPCs and macrophages subjected to different interventions. Flow cytometric analysis revealed that Mito transplantation dose-dependently reduced mitochondrial superoxide levels in ROS-stimulated NPCs (Fig. 4H), as implicated by the reduced fluorescence intensity of MitoSOX, a fluorescence probe for mitochondrial superoxide. This was confirmed by direct fluorescence microscopy observation (Fig. 4I). However, the model and Mito groups showed no significant difference in the total cellular ROS, as indicated by the fluorescence intensity of DCFH-DA (a non-selective fluorescent probe of ROS) in NPCs (Fig. 4J). Similarly, Mito significantly reduced mitochondrial superoxide levels, without affecting total cellular ROS in RAW264.7 macrophages (Fig. S4). In both cases, the best effect was achieved by Mito at 20 × 10^3/mL. These results suggest that Mito transplantation is able to remedy damaged mitochondria in recipient cells, thus inhibiting overproduction of mitochondrial superoxide. Nevertheless, Mito itself cannot eliminate ROS and attenuate ROS-mediation inflammation.

Further studies were conducted to elucidate the mechanisms underlying the biological effects of Mito on mitochondria in transplanted NPCs. Western blot analysis revealed inhibited mitochondrial biogenesis in NPCs of the model group, since the protein level of peroxisome proliferator-activated receptor gamma coactivator 1-alpha (PGC-1α), i.e., a crucial marker of mitochondrial biogenesis, was significantly decreased after ROS stimulation (Fig. 4K). Mito intervention effectively normalized the PGC-1α levels in ROS-stimulated NPCs, indicating restored mitochondrial biogenesis. In addition, we detected increased protein levels of full-length PTEN-induced putative kinase 1 (FL-PINK1) and p62 as well as decreased expression of parkin RBR E3 ubiquitin protein ligase (PRKN) (Fig. 4L–O). In mitochondria with normal MMP, PINK1 is translocated into the inner mitochondrial membrane, where it undergoes rapid degradation. However, in response to mitochondrial damage, PINK1 cannot be properly imported and degraded, leading to the accumulation of FL-PINK1 on the outer mitochondrial membrane. Accumulated PINK1 subsequently recruits and activates the E3 ubiquitin ligase Parkin, which facilitates the ubiquitination of proteins on the mitochondrial outer membrane. Subsequently, the autophagic adaptor protein, such as p62, identifies and binds to the ubiquitinated mitochondria marked by Parkin, promoting their recognition and sequestration by autophagosomes during mitophagy. The adaptor proteins and damaged mitochondria are ultimately degraded through the lysosomal pathway [46]. Consequently, disruption of this homeostatic regulatory mechanism is characterized by decreased Parkin expression and pathological accumulation of p62, resulting from impaired clearance of depolarized mitochondria. Our findings indicate that Mito transplantation can improve mitophagy of NPCs under oxidative conditions. Moreover, we found a significant increase in dynamin-related protein-1 (Drp1) and a decrease in optic atrophy 1 (OPA1) in ROS-induced NPCs (Fig. 4P and Fig. S5). This indicates excessive mitochondrial fission in injured NPCs, as Drp1 is a pro-fission protein [47], while OPA1 functions as a fusion protein [48]. These abnormalities were effectively reversed after treatment with Mito at 20 × 10^3/mL. These results are in accordance with the finding on the average mitochondrial branch length and mitochondrial area (Fig. 4B–C). Accordingly, Mito is also able to regulate mitochondrial dynamics.

Together, these results indicate that Mito can attenuate mitochondrial membrane depolarization, enhance ATP production, and inhibit mitochondrial ROS production in NPCs under pathological conditions, primarily by improving mitochondrial biogenesis, promoting mitophagy, and regulating mitochondrial dynamics.

2.4. Intradiscal treatment with Mito delays the disc degeneration in a rat model of IVDD

Before in vivo therapeutic studies, distribution profiles of Mito after intradiscal injection were examined. First, in vivo fluorescence imaging indicated that DiR-labeled Mito can be retained in the IVD after local injection in the NP tissue of rats (Fig. 5A). Besides, the cryosection of the disc tissue collected at 12 h post intradiscal injection of MTG-labeled Mito was observed by fluorescence microscopy. We found that Mito was mainly distributed in NPCs (Fig. 5B), indicating its cellular internalization in vivo.

Subsequently, we assessed therapeutic effects of Mito in Sprague-Dawley rats with puncture-induced IVDD (Fig. 5C). At week 2 after the first puncture, rats in the model group received PBS, while those in the Mito groups were treated with three distinct doses of Mito per disc to evaluate dose-response effects. The injection doses were calculated based on the number of Mito determined by flow cytometry per milligram of mitochondrial protein. Four weeks after different treatments, X-ray imaging indicated that the disc height index (DHI) of the model group was significantly reduced, as compared to the normal control (Fig. 5D–E). As extensively documented, the decreased disc height is a representative pathological character of IVDD [49]. While treatment with Mito at 7 × 10^4 and 2.1 × 10^5 per disc showed slightly increased DHI values compared to the model group, Mito at 4.2 × 10^5 per disc showed significant improvement. Further magnetic resonance (MR) imaging was conducted for Pfirrmann grade scoring analysis. It was found that discs in the model group displayed considerably inhomogeneous structure and hypointense signals in the NP tissue. These abnormalities were notably mitigated after treatment with Mito at 4.2 × 10^5 per disc (Fig. 5F). Correspondingly, the Pfirrmann grade score of the high-dose Mito group was significantly lower than that of the model group (Fig. 5G).

Histological analyses of IVD sections stained with hematoxylin and eosin (H&E), safranin-O/fast green (SO/FG), or Masson revealed

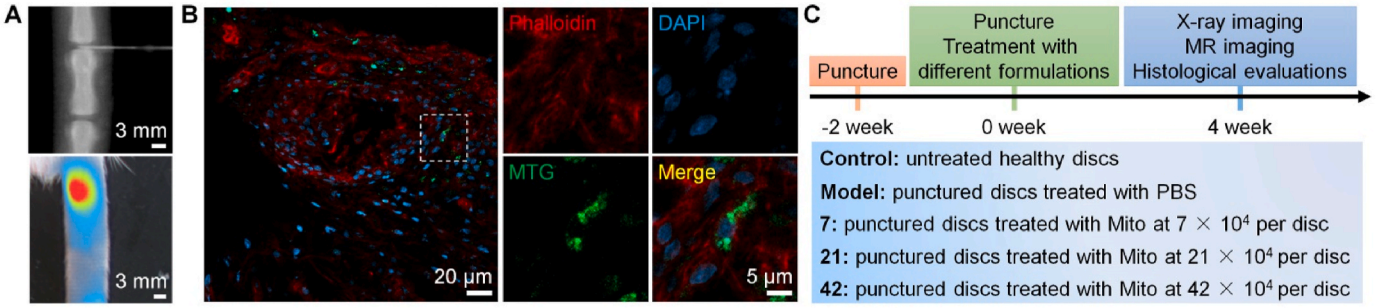

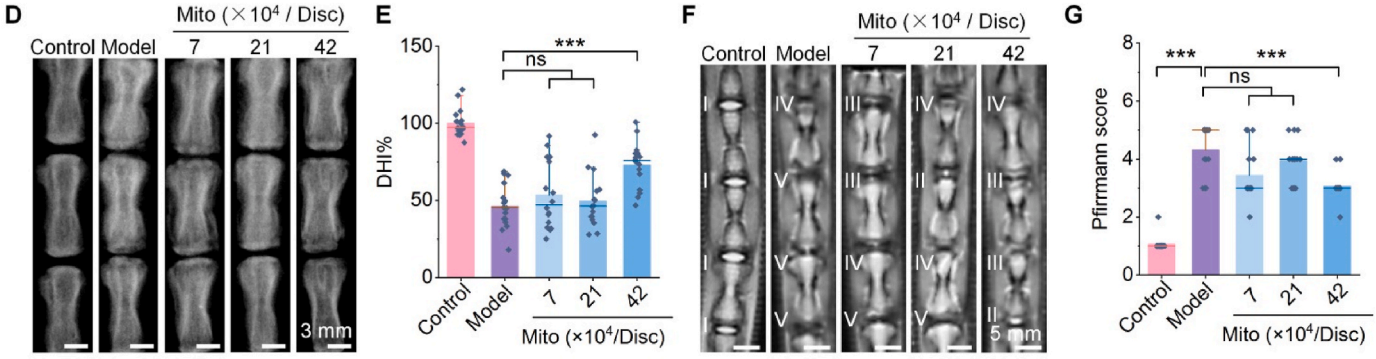

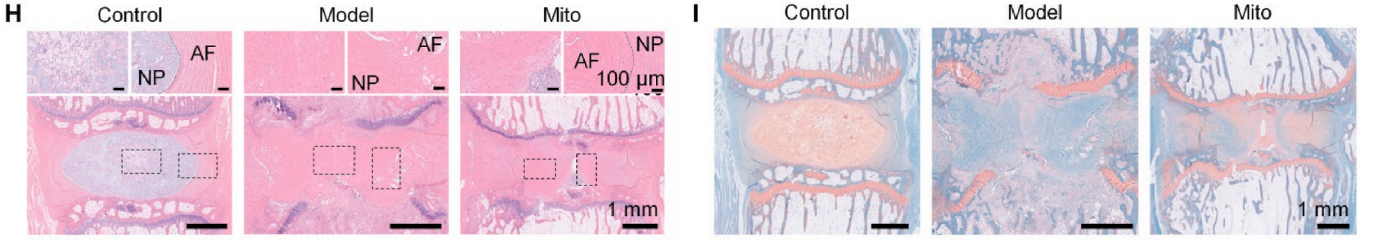

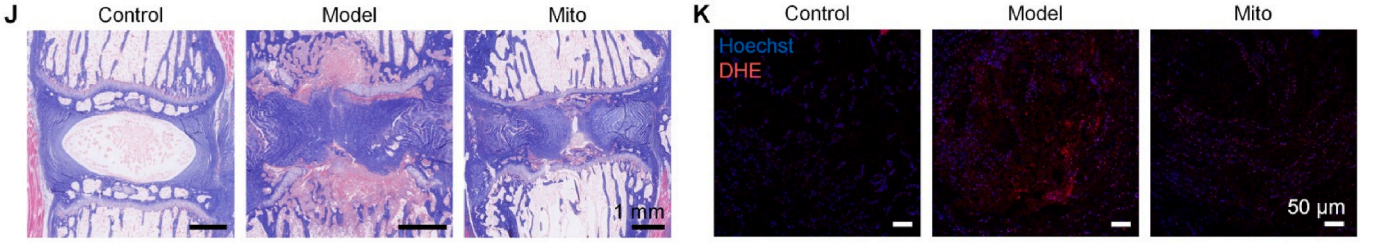

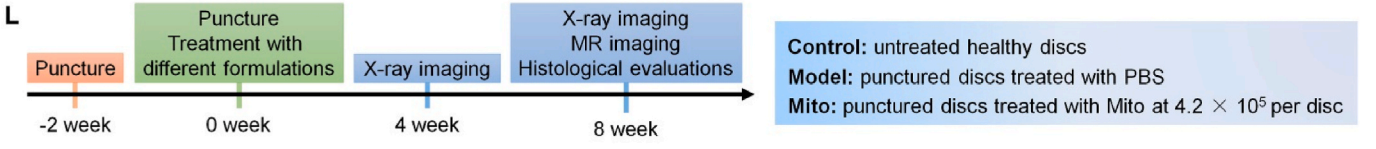

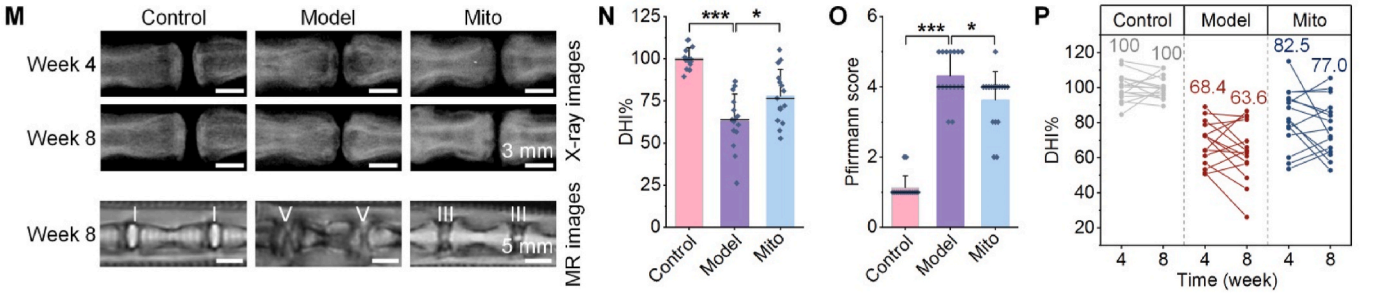

(caption on next page)

Fig. 5. Mito transplantation delays the disc degeneration in a rat model of IVDD. (A) A typical X-ray image acquired upon puncture into the NP tissue (the upper panel) and in vivo fluorescence image indicates local distribution of DiR-labeled Mito after local transplantation via intradiscal injection (the lower panel). (B) CLSM images show transplanted MTG-labeled Mito in the rat disc cryosection. The actin cytoskeleton was stained with Cy3-conjugated phalloidin (red), and nuclei were stained with DPAI. (C) A workflow illustrates the establishment of a rat model of IVDD and treatment procedures for evaluating therapeutic effects. (D–E) Representative X-ray images (D) and calculated DHI values (E) for different groups at week 4 post-treatment (n = 16). (F–G) Representative MR images (F) and Pfirrmann scores (G) for different groups at week 4 after different interventions (n = 16). (H–J) Micrographs of disc sections stained with H&E (H), SO/FG (I), or Masson (J) for various groups. (K) Representative fluorescence images of DHE-stained disc tissue cryosections indicate relative levels of superoxide anion. Nuclei were stained with Hoechst. (L) Treatment procedures for long-term evaluation of in vivo efficacy of transplanted Mito. (M) Representative X-ray and MR images of disc tissues for different groups at two predefined time points. (N–O) Quantification of DHI values (n = 15) and Pfirrmann scores (n = 16) at week 8 post-treatment. (P) Quantitative analysis of DHI changes at weeks 4 and 8 after various interventions (n = 15). Data are presented as means ± SD. Statistical differences were analyzed using the one-way ANOVA with posthoc LSD or Tamhane's tests. *P < 0.05 and ***P < 0.001; ns, no significance.

disorganized IVD structures in the model group, characterized by an unclear boundary between the NP and AF tissues, along with the ruptured cartilage endplate and abnormal deposition of fibrosis-related collagen (Fig. 5H–J). After treatment with Mito for 4 weeks, H&E staining showed that remodeling of IVD tissue structures was considerably mitigated, as evidenced by reduced histological scores (Fig. S6A). Consistently, the ECM in the NP area exhibited a higher content of proteoglycans with a decreased collagen volume fraction (CVF), as indicated by SO/FG and Masson staining of the Mito group (Fig. 5I–J and Fig. S6B). Consistent with these structural improvements in NP tissues, examination of cryosections stained with dihydroethidium (DHE), i.e., a fluorescent probe of superoxide, indicated that Mito therapy significantly decreased ROS levels in the IVD tissues (Fig. 5K and Fig. S7A), most likely resulting from reduced superoxide leakage from the complexes of the mitochondrial ETC. This is in line with the in vitro finding that transplanted Mito can effectively reduce mitochondrial superoxide levels through mitochondrial revitalization.

In view of the improved disc structure at week 4 after Mito treatment, we further investigated whether the transplanted Mito can reverse the pathogenic degenerative process following long-term treatment (Fig. 5L). In this case, Mito at 4.2×10^5 per disc was examined. After 8 weeks of treatment, X-ray imaging revealed that the Mito group exhibited a significantly higher DHI than the model group (Fig. 5M − N). Likewise, analysis of MR images showed significantly reduced Pfirrmann scores in the Mito group (Fig. 5M and O). Additionally, quantitative analysis of X-ray images acquired at two time points indicated that the DHI value for the model group at week 8 showed no significant reduction compared to that at week 4 (Fig. 5P). This suggests that the degree of degeneration in the IVD at week 4 was already quite severe, with no substantial progression over the following 4 weeks. In contrast to PBS-treated IVDD rats in the model group, Mito treatment effectively mitigated IVDD, as evidenced by significantly enhanced DHI values at both weeks 4 and 8. Furthermore, no significant difference was observed between the DHI values at these two time points for the Mito group, indicating that the therapeutic benefit achieved with Mito at week 4 was maintained over the subsequent 4 weeks. Of note, the Mito group showed a remarkably lower level of superoxide in the IVD at week 8 compared to the model group, as indicated by the weaker DHE fluorescence (Fig. S7B). Consequently, these results demonstrate that either short- or long-term treatment with Mito via intradiscal injection can effectively delay puncture-induced IVDD in rats, primarily by regulating mitochondrial homeostasis of NPCs and alleviating the pathological abnormalities in the IVD.

2.5. Engineering of Mito with a mitochondrial-targeting bioactive macromolecule

Whereas the above findings demonstrate that Mito transplantation is able to delay disc degeneration in rats, this treatment option does not halt the pathogenic process or reverse it by promoting regeneration. In particular, we did not observe a restoration of the NP structure with the typical gelatinous appearance, which is essential for absorbing axial compression of body and maintaining spinal connectivity [50]. Therefore, therapeutic effects of the Mito therapy remain to be enhanced. We further analyzed the scRNA-seq data derived from human samples to identify additional key factors dominating the progression of IVDD. Gene set enrichment analysis (GSEA) revealed that the DEGs between fibrochondrocytes and homeostatic NPCs were significantly enriched for pathways associated with oxidative stress, lipid oxidation, leukocyte transendothelial migration, and inflammatory response (Fig. 6A–C). Consistently, we detected increased expression levels of thioredoxin-interacting protein (TXNIP, a key protein relevant to cellular oxidation), superoxide, TNF-α, and IL-1β in the degenerated rat IVD tissues (Fig. 6D–E). These results suggest that exacerbated oxidative stress and inflammation also play a critical role in the progression of IVDD. However, intervention with Mito alone cannot fully address all of these pathologically relevant factors, as it primarily facilitates mitochondrial homeostasis and partially attenuates mitochondrial ROS by reducing superoxide generation. Accordingly, we propose our second hypothesis that the combination of Mito with antioxidative and anti-inflammatory therapies may serve as a more promising treatment option for IVDD.

In light of this, we designed a multifunctional macromolecular therapy, referred to as PSP (Fig. 1A), which is derived from 8-arm polyethylene glycol (8PEG) simultaneously conjugated with a mitochondrial-targeting peptide SS31 and seven bioactive modules of phenylboronic acid pinacol ester (PBE) (Fig. S8A). Of note, our previous studies have demonstrated that the PBE-containing materials exhibit strong antioxidative and anti-inflammatory activities in different animal models of acute and chronic inflammatory diseases [51–53]. The successful synthesis of PSP was structurally confirmed by Fourier transform infrared (FTIR), ^{1}H NMR, and matrix-assisted laser desorption/ionization time-of-flight (MALDI-TOF) mass spectrometry (Figs. S8B–D). FTIR analysis revealed hydroxyl and N-H stretching peaks around 3500 cm^{-1}, C=O absorption at 1752 cm^{-1} for ester or amide bonds, a benzene ring peak at 1677 cm^{-1}, and a B-O stretching peak at 1347 cm^{-1}. Correspondingly, the ^{1}H NMR spectrum confirmed the incorporation of PBE and SS31 moieties within PSP, as evidenced by the distinct proton signals due to methyl and phenyl groups in PBE and SS31. In addition, calculation based on the proton signals in the ^{1}H NMR spectrum indicated that each PSP conjugate contained approximately one 8PEG, seven PBE units, and one SS31 peptide. Following similar procedures (Fig. S9A), Cy5-labeled PSP (Cy5-PSP) was synthesized and characterized by ^{1}H NMR, ultraviolet–visible, and fluorescence spectroscopy (Figs. S9B–D).

In vitro tests showed that PSP effectively eliminated 2,2-diphenyl-1-picrylhydrazyl radical (DPPH•), superoxide anion ($\bullet O_2^-$), and H_2O_2 (Figs. S10A–C), indicating its ability to scavenge different types of ROS. In addition, PSP significantly inhibited the expression of TNF-α in H_2O_2-stimulated macrophages in a dose-dependent manner (Fig. S10D). These results confirmed antioxidative and anti-inflammatory activities of PSP. Leveraging the mitochondrial-targeting capability of SS31 in PSP, Mito can be easily engineered with PSP through simple co-incubation in an aqueous solution (Fig. 6F and Fig. S11A). To prepare PSP-functionalized Mito (i.e., Mito-PB) with varying PSP contents, different PSP/Mito weight ratios were used. Similarly, Mito was decorated with Cy5-PSP to afford Cy5-Mito-PB for fluorescence imaging studies. Flow cytometric quantification revealed an increase in Cy5 fluorescence as the Cy5-PSP/

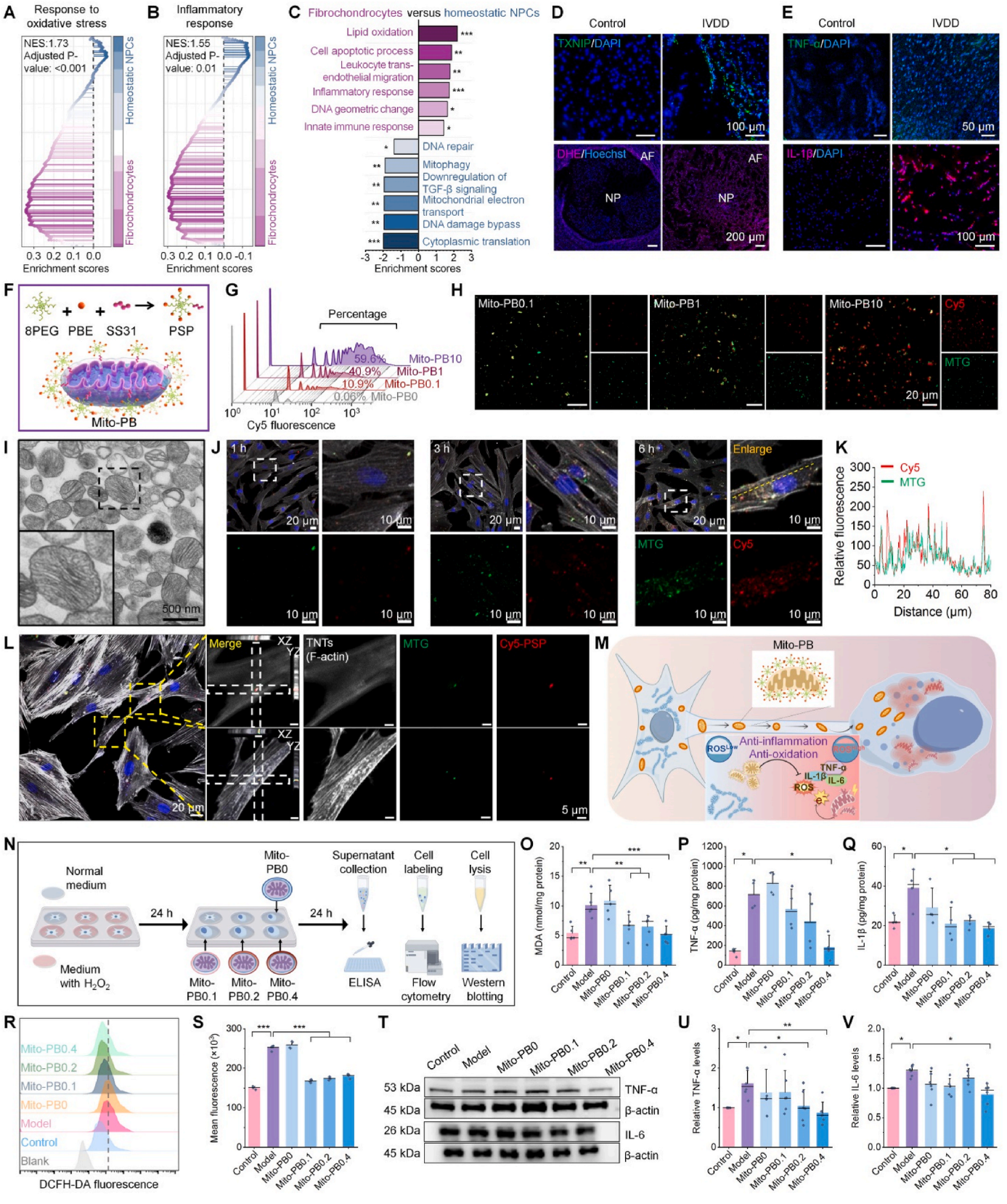

(caption on next page)

Fig. 6. Rational engineering of Mito with a mitochondrial-targeting bioactive macromolecule and in vitro evaluation of biological effects. (A–C) GSEA of DEGs among fibrochondrocytes and homeostatic NPCs indicates oxidative stress (A), inflammatory response (B), and other enriched biological processes such as lipid oxidation and cell apoptosis (C). (D) Fluorescence images show high expressions of TXNIP (green) and ROS (red) in cryosections of the degenerated rat discs. (E) Immunofluorescence analysis of the expression levels of TNF-α (green) and IL-1β (red) in cryosections of the normal and degenerated rat discs. (F) Schematic illustration of PSP and PSP-functionalized Mito (Mito-PB). (G–H) Typical flow cytometric curves (G) and fluorescence images (H) demonstrate increased loading of Cy5-PSP onto Mito as the Cy5-PSP/Mito weight ratio varied from 0.1:6, 1:6, to 10:6. (I) Representative TEM image of Mito-PB. (J) Fluorescence images showing time-dependent internalization of Cy5-labeled Mito-PB in NPCs. The regions delineated by the white dashed boxes are magnified and displayed as merged fluorescence images, along with separate channels for MTG and Cy5 fluorescence. (K) The co-localization profile of the Cy5 fluorescence signal of Cy5-PSP (red) with Mito (green) at the indicated region in NPCs. (L) Z-stack scanning images indicate intercellular transfer of Mito-PB among NPCs through TNTs. Red, Cy5-PSP; grey, Cy3-labeled F-actin; green, MTG-stained Mito-PB. (M) A sketch illustrates intercellular transfer of Mito-PB via TNTs to realize antioxidative and anti-inflammatory effects across NPCs. (N) A diagram shows Mito-PB treatment procedures for in vitro evaluation of biological effects of Mito-PB in NPCs. In the control group, cells were treated with the medium alone, while the model group was induced with H_2O_2, followed by intervention with fresh medium alone. Cells in the Mito-PB groups were treated with ROS and Mito-PB containing different contents of PSP. (O–Q) Quantified levels of MDA (O, n = 5), TNF-α (P, n = 4), and IL-1β (Q, n = 4) in NPCs after indicated treatments. (R–S) Flow cytometric curves (R) and quantitative analysis (S) of total cellular ROS levels in macrophages (n = 4). (T–V) Typical Western blot bands (T) and quantification of TNF-α (U) and IL-6 (V) levels in macrophages (n = 6). Images in (F, M, N) were created with Figdraw.com. Data are presented as means ± SD. Statistical differences were determined using the one-way ANOVA with posthoc LSD or Tamhane's tests. *P < 0.05, **P < 0.01, and ***P < 0.001.

Mito weight ratio varied from 0:6, to 0.1:6, 1:6, and 10:6, indicating enhanced decoration of Cy5-PSP on Mito (Fig. 6G). This was further confirmed by fluorescence observation via CLSM (Fig. 6H). Moreover, fluorescence images showed notable co-localization of the red fluorescence from Cy5-PSP with the green fluorescence from MTG-labeled Mito, indicating effective binding of Cy5-PSP to Mito. TEM observation showed that Mito-PB maintained the shape and morphology similar to those of Mito (Fig. 6I). Nevertheless, the TEM images of Mito-PB revealed a denser peripheral structure, mainly due to the PSP coating. DLS measurement revealed a slight increase in the mean diameter of Mito after PSP decoration. For Mito-PB with PSP/Mito weight ratios of 0.1:6, 1:6, and 10:6, i.e., Mito-PB0.1, Mito-PB1, and Mito-PB10, the mean sizes were 717, 729, and 755 nm, respectively (Fig. S11B), with negative ζ-potential for all Mito-PBs (Fig. S11C). The calculated binding efficiency of PSP to Mito was approximately 59.7 %. To assess the binding stability of PSP on Mito, in vitro dissociation tests were conducted. After Cy5-Mito-PB was incubated in PBS for various time periods, we observed no increase in the fluorescence intensities of the collected supernatant (Fig. S12A). These results evidence that Mito can be successfully engineered with PSP, and the PSP content in the resulting Mito-PB may be easily tailored by modulating the feeding ratio of PSP to Mito. Importantly, Mito-PB displayed excellent stability during long-term storage in PBS.

2.6. Cellular uptake and biological activity of Mito-PB

Similar to Mito, Cy5-Mito-PB showed a time-dependent cellular uptake profile in NPCs (Fig. 6J). At 1, 3, and 6 h after incubation of Cy5-Mito-PB in NPCs, the red fluorescence from Cy5-PSP exhibited significant co-localization with the green fluorescence from MTG-labeled Mito (Fig. 6J–K). Even 24 h post-incubation with Mito-PB dual-labeled with Cy5 and MTG, NPCs maintained remarkable co-localization of Cy5 and MTG fluorescence signals (Fig. S12B). Furthermore, histological analysis of the disc tissue at 24 h post-intradiscal injection of Cy5/MTG-labeled Mito revealed substantial spatial overlap between red and green fluorescence signals in NPCs (Fig. S12C). These consistent observations from both in vitro and in vivo experiments demonstrate the exceptional stability of Mito-PB following cellular internalization in NPCs, corroborating the finding from our in vitro stability assessment (Fig. S12A). Moreover, we observed considerable co-localization of the Cy5 and MTG fluorescence signals in TNTs of NPCs at 24 h post-incubation (Fig. 6L), implying that PSP on Mito-PB can be transferred between cells through TNTs via a hitchhiking effect, thereby facilitating desirable antioxidative and anti-inflammatory effects across different cells (Fig. 6M).

Then biological effects of Mito-PB were evaluated in both NPCs and macrophages (Fig. 6N). As anticipated, ROS-induced NPCs displayed markedly elevated levels of characteristic oxidative and pro-inflammatory mediators, including malondialdehyde (MDA), TNF-α, and IL-1β, coupled with significantly reduced levels of the anti-inflammatory cytokine IL-10 (Fig. 6O–Q and Fig. S13). Notably, Mito-PB treatment effectively normalized their levels in a dose-dependent manner based on the PSP content. Similarly, Mito-PB demonstrated antioxidative and anti-inflammatory activities in macrophages (Fig. 6R–V). Among the tested formulations, the most pronounced therapeutic effect was observed for Mito-PB0.4 (Mito-PB with a PSP/Mito weight ratio of 0.4:6). In addition, these results confirmed that Mito alone showed limited capacity to mitigate oxidative stress and inflammation in both NPCs and macrophages.

Collectively, our findings demonstrate that the decoration of Mito with PSP preserves its inherent cellular internalization properties. Importantly, engineering with PSP significantly enhances the bioactivities of Mito. Beyond exerting biological effects in internalized cells, the Mito-mediated transfer of Mito-PB between cells facilitates antioxidation and inflammation-resolving functions in neighboring standby cells, thereby amplifying therapeutic benefits. Consequently, Mito-PB has the potential to serve as a powerful biotherapy for addressing oxidative stress and pro-inflammatory processes associated with pathogenic disc degeneration, offering a novel approach to modulating these detrimental conditions.

2.7. Mito-PB ameliorates IVDD in rats

Subsequently, we evaluated in vivo therapeutic effects of Mito-PB. A needle-punctured disc degeneration model was established following the previously described procedures. Two weeks after puncture, rats were treated with PBS or 4.2×10^5 Mito-PB containing various contents of PSP, specifically Mito-PB0, Mito-PB0.1, Mito-PB1, and Mito-PB10, via intradiscal injection into each disc (Fig. 7A). X-ray and MR imaging was performed at week 4 following different treatments. The results indicated that all Mito-PB treatment groups exhibited significantly higher DHI values compared to the PBS-treated model group (Fig. 7B–C). Furthermore, MR imaging revealed effectively reduced Pfirrmann scores post treatment with Mito-PB (Fig. 7D). The most effective outcome was achieved with Mito-PB1, which showed significant improvement compared to Mito-PB0, i.e., Mito without PSP decoration. It is worth noting that several discs from different rats treated with Mito-PB1 displayed bright white NP tissues with hyperintensities in MR images, along with a clear delineation between NP and AF tissues (Fig. 7B and Fig. S14). Consistently, histological analysis of IVD sections stained with either SO/FG or Masson revealed that the discs from the Mito-PB1 group were enriched in proteoglycans compared to fibrotic collagen components, as evidenced by the lowest histological score and CVF value among all IVDD groups (Fig. 7E–H). Additionally, the IVDs treated with Mito-PB1 exhibited more normal gelatinous structures in the NP tissues, with fewer ruptured fibers in the AF and showing distinct borders between the NP and AF tissues.

Considering the favorable radiological outcomes achieved with Mito-PB1, its beneficial effects on mitochondrial function and the

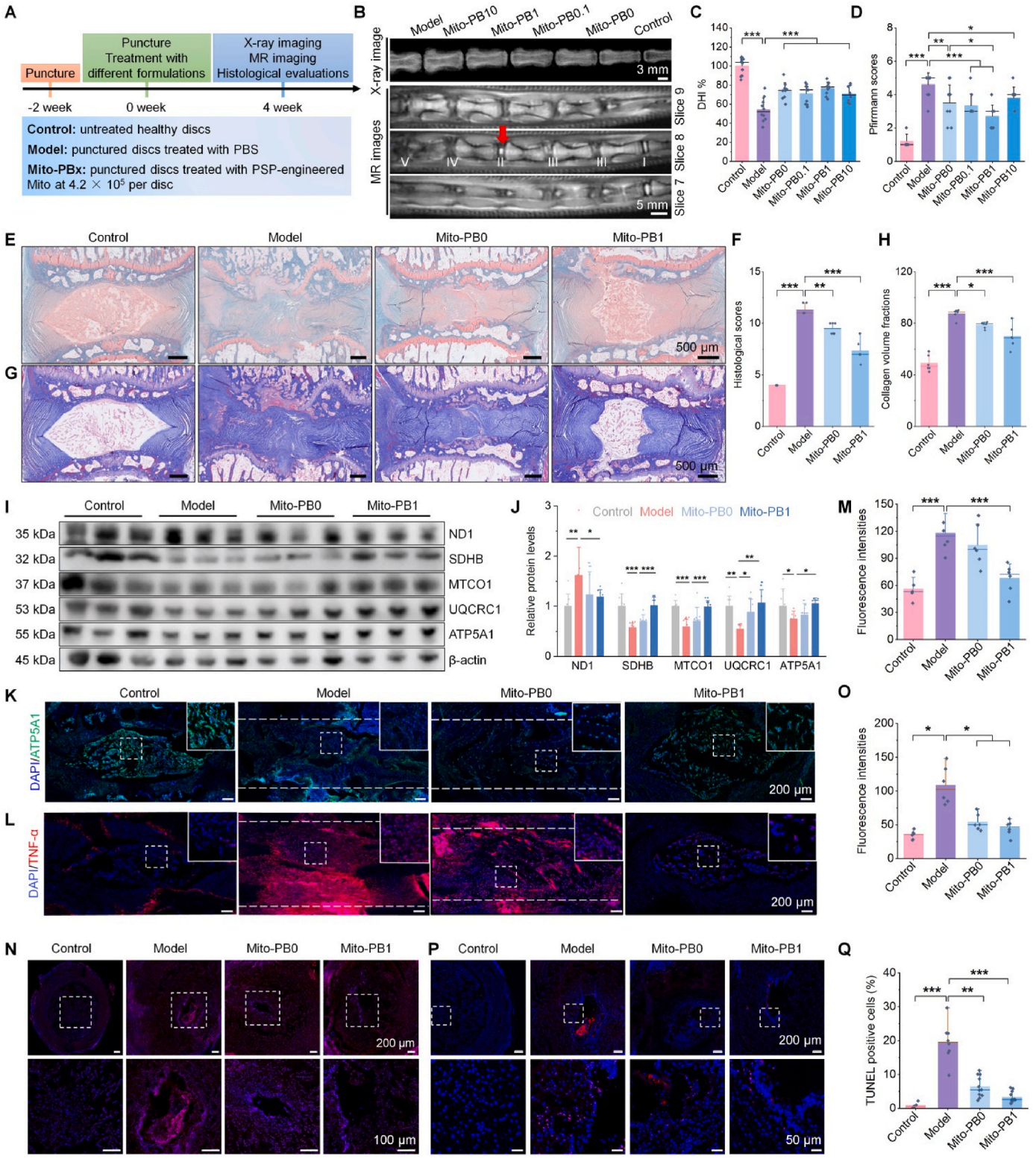

Fig. 7. Mito-PB ameliorates IVDD in rats by its multiple bioactivities. (A) A workflow illustrates treatment procedures. (B–D) Representative X-ray and MR images (B) as well as analysis of DHI values (C) and Pfirrmann scores (D) in different groups at week 4 after different interventions (n = 10). (E–H) Micrographs of disc tissue sections stained with SO/FG (E) or Masson (G) as well as the quantified histological scores (F) and collagen volume fractions (H) for different groups (n = 6). (I–J) Western blot analysis of relative protein levels of ND1, SDHB, MTCO1, UQCRC1, and ATP5A1 in rat disc tissues (n = 8). (K–L) Immunofluorescence images show relative expression levels of ATP5A1 (K) and TNF-α (L) in the disc tissues. (M) Quantitative analysis of relative TNF-α levels (n = 5–6). (N–O) Representative fluorescence images of DHE-stained cryosections of rat disc tissues (N) and quantification of superoxide anion levels (O) (n = 6). (P–Q) Fluorescence images of TUNEL-stained rat disc sections (P) and quantitative analysis of apoptotic cells (Q, n ≥ 6). Data are presented as means ± SD. Statistical differences were determined using the one-way ANOVA with posthoc LSD or Tamhane's tests. *P < 0.05, **P < 0.01, and ***P < 0.001; ns, no significance.

pathological microenvironment in the IVD tissues were further evaluated. We analyzed the expression levels of OXPHOS proteins, including ND1, SDHB, MTCO1, UQCRC1, and ATP5A1, which are critical components of mitochondrial complexes I, II, III, IV, and V, respectively. The results showed that ND1 levels were significantly elevated, while SDHB, MTCO1, UQCRC1, and ATP5A1 levels were markedly reduced in the model group (Fig. 7I–J), suggesting a disruption of the mitochondrial ETC. Abnormalities in mitochondrial complex activities can shift the ETC towards the RET pathway, leading to a transition from the ATP production to excessive superoxide generation and inflammation [54]. Unlike the other inhibited complex subunits observed during degeneration, the upregulated activity of mitochondrial complex I may promote RET and exacerbate mitochondrial dysfunction [55]. Treatment with Mito therapies, particularly Mito-PB1, effectively normalized the expression levels of these OXPHOS proteins. Furthermore, immunofluorescence analysis of disc cryosections confirmed the altered ATP5A1 expression across different groups (Fig. 7K). These results indicate that Mito-PB1 treatment restores mitochondrial homeostasis and promotes function recovery. In accordance with the beneficial outcomes, histological analyses further revealed significant inhibition of inflammation and attenuation of oxidative stress following Mito-PB1 therapy, as implicated by markedly decreased levels of TNF-α and ROS in the cryosections of degenerated discs (Fig. 7L–O). Correspondingly, TUNEL staining demonstrated that Mito-PB1 effectively reduced cell apoptosis in the NP tissue (Fig. 7P–Q), while severe cell apoptosis was observed in the model group. Also, immunohistochemistry analysis showed a substantial decrease in the expression of Tie2, a marker of NP progenitor cells, in the degenerated IVD tissue (Fig. S15). This observation aligns with previous studies demonstrating that Tie2 expression is significantly diminished during aging and IVDD progression, which correlates with a compromised regenerative potential of the disc [56]. Notably, treatment with Mito-PB markedly upregulated Tie2 expression, suggesting a restoration of the regenerative capacity of NPCs in the IVD.

Taken together, our results demonstrate that engineering Mito with the macromolecular therapy PSP can significantly enhance its therapeutic effects on IVDD. In addition to notably restoring the normal NP structure, Mito-PB intervention effectively recovered mitochondrial function and OXPHOS activity, normalized the pathological microenvironment, and inhibited abnormal cell apoptosis in degenerated IVDs. This potentiated efficacy is primarily attributed to the antioxidative and anti-inflammatory properties introduced through PSP functionalization.

2.8. Mechanistic studies on therapeutic effects of Mito-PB

2.8.1. The fibrosis-related protein SPARC mediates detrimental inflammation and mitochondrial damage during IVDD via STING signaling

On the basis of the above promising findings, we further explored the mechanisms underlying therapeutic effects of Mito-PB on IVDD. Gene co-expression plots derived from scRNA-seq data identified that NPCs with high levels of COL1A1 ($COL1A1^{High}$, labeled in red) were primarily associated with elevated expression of secreted protein acidic and rich in cysteine ($SPARC^{High}$, labeled in blue), resulting in a subset of NPCs labeled as $COL1A1^{High}SPARC^{High}$ NPCs (pink). Importantly, $COL1A1^{High}SPARC^{High}$ NPCs predominantly belonged to the fibrochondrocyte population (Fig. 8A). Notably, SPARC expression levels increased in accordance with the severity of disc degeneration (Fig. 8B). Moreover, correlation analysis revealed that SPARC expression levels were positively associated with several genes implicated in fibrosis (Fig. S16A). These findings suggest that SPARC plays a critical role in fibrosis during IVDD. Additionally, we found that the expression level of SPARC was negatively correlated with the OXPHOS activity of NPCs, showing a robust correlation coefficient of −0.56 (Fig. 8C). Conversely, SPARC expression was positively correlated with glycolytic activity, with a correlation coefficient of 0.48 (Fig. 8D). These results indicate that SPARC may be involved in mitochondrial damage associated with aging and degeneration, consistent with a recent study on age-related inflammation [57]. Furthermore, immunofluorescence analysis of rat disc cryosections confirmed that the upregulation of SPARC correlates with disc degeneration (Fig. 8E).

As a pro-inflammatory and fibrosis-related protein, elevated secretion of SPARC from adipose tissues has been shown to be associated with the activation of inflammation and interferon response in macrophages. This process is mediated by the direct interaction between SPARC and toll-like receptor-4 (TLR4) [57], a key member of TLR family that is critical for the innate immune response. In addition to TLR4, our molecular docking results indicate that SPARC can effectively bind to several intracellular immune sensor proteins, including MD2, STING, NLRP3, P2X7, MAVS, and ZBP1 (Fig. S16B). In particular, a minimal binding energy of −302.6 kJ/mol was calculated for the interaction between SPARC and STING (Fig. 8F and Fig. S16B). Moreover, immunofluorescence analysis revealed co-localization of SPARC and STING in both NPCs and disc sections (Fig. 8G–H). Further, we conducted Western blot analysis of immunoprecipitation (IP-Western) to identify the coprecipitated proteins in degenerated disc tissues, and the result confirmed a strong interaction between SPARC and STING (Fig. 8I). Consistently, biolayer interferometry (BLI) measurement demonstrated a direct interaction of SPARC with STING in a concentration-dependent manner, with a dissociation constant (KD) of 3.0×10^{-12} M (Fig. 8J–K). Collectively, these results imply that the fibrosis-related protein SPARC may contribute to detrimental inflammation and mitochondrial damage during IVDD, by specifically engaging STING signaling.

2.8.2. Mito-PB alleviates IVDD by regulating the mtDNA/SPARC-STING axis

To confirm the SPARC-STING axis mediating efficacies of Mito-PB, different molecules involved in this signaling pathway were determined. As well documented, mitochondrial DNA (mtDNA) can be released into the cytoplasm in response to cellular stress, mainly resulting from mitochondrial dysfunction [33]. Cytosolic mtDNA can activate the STING pathway by cyclic GMP-AMP synthase (cGAS) [58]. Therefore, we first detected the levels of mtDNA in NPCs following different treatments. Quantification via qPCR, utilizing primers specific to either the non-coding D-Loop region or the coding MT-ND1 region, revealed significantly elevated expressions of cytosolic mtDNA in ROS-stimulated NPCs compared to normal NPCs (Fig. 9A–B). Treatment with either Mito-PB0 or Mito-PB0.4 effectively normalized cytosolic mRNA levels to those comparable to the normal control.

Consistent with the above findings, Western blot assay revealed significantly higher expression of SPARC in ROS-stimulated NPCs, which was markedly reduced after treatment with Mito-PB0.4 (Fig. 9C–D). In IVD tissues from rats, we also detected significantly lower expressions of SPARC in the Mito-PB1 group, as compared to the model group (Fig. S17). Also, we found that the model group exhibited high levels of phosphorylated STING (p-STING) and phosphorylated TBK1 (p-TBK1) in ROS-stimulated NPCs (Fig. 9C and 9E–F), indicating activation of STING signaling and subsequent inflammatory responses in this case [59]. Mito-PB0.4 treatment markedly reduced the expression levels of p-STING and p-TBK1. Notably, the relative levels of p-STING/STING and p-TBK1/TBK1 in the Mito-PB0.4 group were even comparable to PBS-treated NPCs in the control group. Proximity ligation assay (PLA) was further performed to verify the in situ physical interaction between SPARC and STING, as well as quantify their interacting intensities in NPCs after different interventions. Stronger fluorescence signals from SPARC and STING were observed in NPCs stimulated with ROS (Fig. 9G–H). In contrast, Mito-PB0.4 treatment significantly reduced the corresponding fluorescence intensity. These results indicate that the interaction between SPARC and STING is enhanced under oxidative conditions, which was effectively diminished following Mito-PB0.4 treatment, concomitant with decreased SPARC production.

Moreover, it was found that Mito-PB0.4 treatment remarkably reduced the expressions of NLRP3, cleaved caspase-1, and IL-1β (Fig. 9I), indicating that this mitochondrial-derived biotherapy can attenuate the

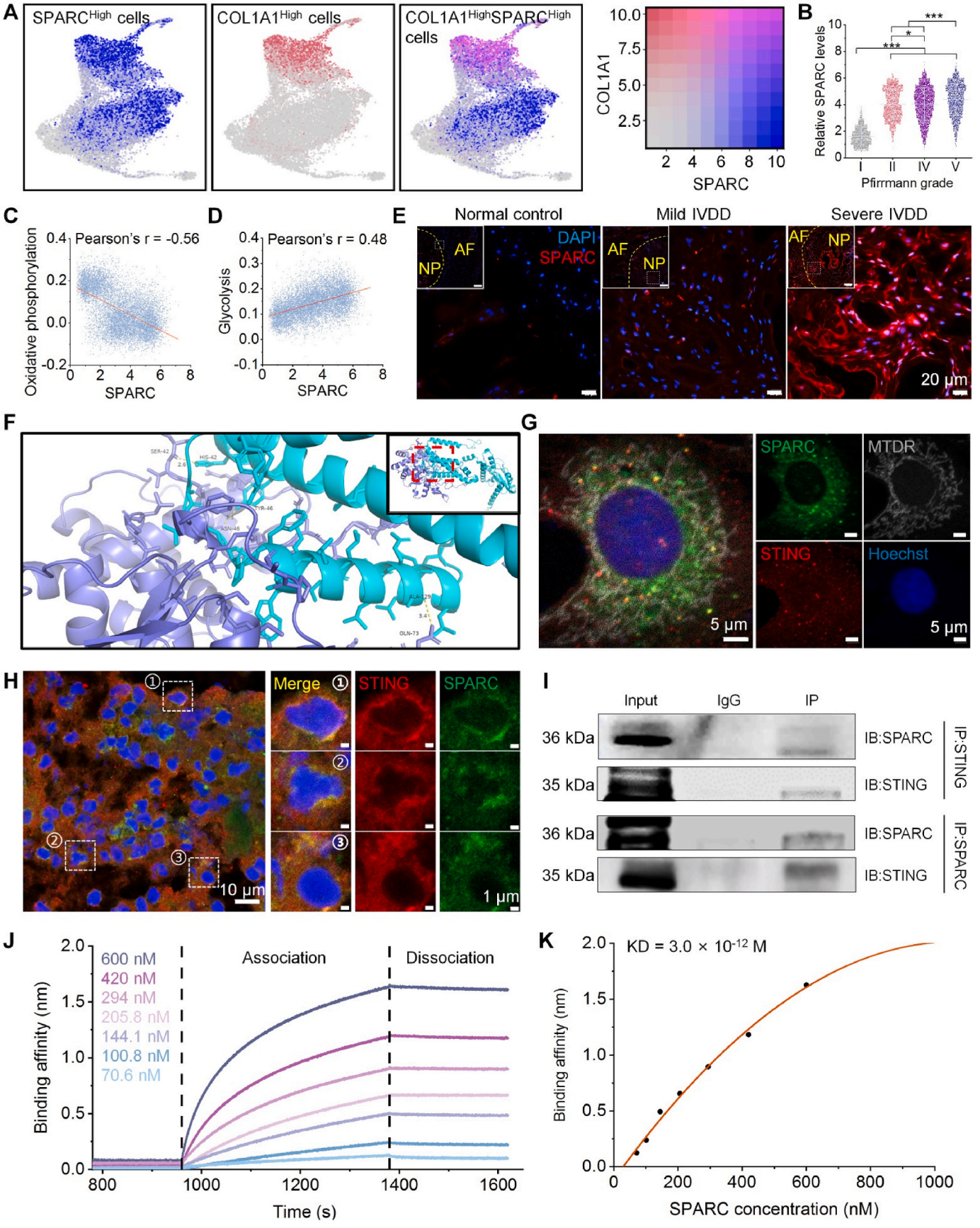

(caption on next page)

Fig. 8. Fibrosis-related protein SPARC mediates inflammation and mitochondrial damage during IVDD by interacting with STING. (A) ScRNA-seq data reveals evident co-expression of SPARC and COL1A1 in the human NP tissues. The UMAP images in the left and middle panels show gene expressions of SPARC and a fibrosis-related collagen COL1A1, respectively. The blended UMAP plot in the right panel indicates the co-expression of SPARC and COL1A1, evidently in the fibrochondrocyte subcluster. The grey color indicates low expression levels of related genes, while the red and blue colors represent their high expression. (B) Analysis of scRNA-seq data indicates SPARC expressions in the human NP tissues with various Pfirrmann grading scores. (C–D) Correlation scatter plots of SPARC with oxidative phosphorylation (C) and glycolysis (D) based on scRNA-seq data of human NP tissues. (E) Immunofluorescence images show relative SPARC levels in cryosections of rat disc tissues with different degeneration degrees. (F) Molecular docking illustrates strong interaction between SPARC and STING. (G) Immunofluorescence images of rat NPCs reveal co-localization of SPARC (green) with STING (red). Mitochondria were labeled with MTDR, while nuclei were stained with Hoechst. (H) Immunofluorescence images of rat disc cryosections show localization of green fluorescence from SPARC with red fluorescence due to STING. (I) Co-immunoprecipitation assay verifies the interaction between SPARC and STING in the degenerated rat disc tissue. (J–K) BLI analysis of the SPARC concentration-dependent association and dissociation kinetics of SPARC and STING. (K) The SPARC concentration-dependent binding affinity and dissociation equilibrium constant. Data in (B) are presented as means ± SD. Statistical differences were analyzed using the one-way ANOVA with posthoc LSD or Tamhane's tests. *$P < 0.05$ and ***$P < 0.001$.

NLRP3 inflammasome-mediated inflammatory responses. In combination with decreased STING after Mito-PB0.4 therapy, our results agree with the previous findings that STING can activate the NLRP3 inflammasome, which further facilitates the autocatalytic cleavage of pro-caspase-1 into cleaved caspase-1 and promotes IL-1β release, thereby mediating recruitment of immune cells and production of other pro-inflammatory cytokines [1]. In accordance with inflammation resolution following Mito-PB0.4 therapy, the expression of 8-hydroxy-2′-deoxyguanosine (8-OHdG), a critical biomarker of oxidative damage to DNA, was also significantly reduced in the Mito-PB0.4 group (Fig. 9J).

Meanwhile, normal expression of collagen type II (COLII) is essential for the structural integrity and function of the IVD [60]. However, the degenerated IVDs often display a marked decrease in the expression and synthesis of COLII, mainly resulting from inhibited expression and promoted catabolism of COLII by inflammatory cytokines [1]. Consistently, both ROS-induced NPCs and the degenerated IVD tissues exhibited significantly lower levels of COLII, while its expression was reversed after treatment with Mito-PB (Fig. 9K–N). Overall, these results demonstrate that Mito-PB can effectively inhibit the activation of the ROS-mediated NF-κB pathway and prevent the release of mtDNA from damaged mitochondria, ultimately regulating the STING signaling pathway in both NPCs and degenerated IVDs. The down-regulation of this signaling pathway further promotes mitochondrial homeostasis, inhibits inflammatory responses, reduces oxidative damage, and facilitates the recovery of both the structure and function of the IVD (Fig. 9O).

2.9. Safety evaluations of Mito-PB

Finally, we assessed potential adverse effects of Mito therapies in rats two weeks after intradiscal injection of Mito-PB0 or Mito-PB1 at 7×10^5 per disc. Histopathological examination of H&E-stained sections from major organs (including the heart, liver, spleen, lung, and kidney) of treated rats revealed no detectable tissue injuries or pathological abnormalities (Fig. S18A). Consistently, serum levels of biomarkers associated with hepatic and renal functions remained within normal ranges, showing no significant differences between the control and Mito therapy groups (Fig. S18B). Overall, these preliminary results suggest that intradiscal administration of Mito therapies, even at a dose significantly exceeding those used in therapeutic studies, did not induce observable systemic toxicity. This finding is in agreement with previous reports indicating that mitochondrial transplantation is well-tolerated and does not trigger inflammatory responses or immune rejection [61].

3. Discussion

During the aging process, the degeneration of NP tissues has been recognized as a primary etiological factor underlying IVDD. Dysfunctional and impaired mitochondria are frequently associated with ECM remodeling and fibrosis in affected regions across various diseases [26,31,62]. Notably, fibrosis of the gelatinous NP tissues constitutes a prevalent pathogenic manifestation in IVDD progression [2,4,10,63]. As the central hub for redox reactions, mitochondria are particularly vulnerable to oxidative stress, which can trigger a cascade of detrimental effects, including exacerbated inflammation, DNA damage, and cell apoptosis, ultimately accelerating disc degeneration [28,64]. Consequently, therapeutic strategies aimed at mitigating oxidative stress and restoring mitochondrial function present promising avenues for IVDD treatment. Recently, accumulating evidence has highlighted the therapeutic potential of mitochondrial function restoration in the management of IVDD. In addition to molecular agents capable of modulating mitochondrial activity [65,66], emerging therapeutic approaches, including cell-derived therapies, rationally designed delivery systems, and specifically engineered mitochondrial-targeting biomaterials, have demonstrated significant mitochondrial protective effects in IVDD treatment [19,67–70].

In contrast to these mitochondrial-regulating strategies, mitochondrial transfer represents an innovative therapeutic approach that distinguishes itself from traditional mitochondrial interventions [33,71]. This method, particularly when combined with rational engineering, offers multiple therapeutic advantages. By directly delivering functional mitochondria to compromised cells, it enables rapid restoration of cellular energy metabolism, thereby enhancing cellular function within a relatively shorter timeframe compared to conventional methods. This capacity to augment energy metabolism not only improves cellular performance but also potentiates the regenerative and reparative capabilities of recipient cells, which is particularly important in the treatment of degenerative bone and joint diseases. Furthermore, mitochondrial transplantation demonstrates superior safety profiles relative to certain delivery systems or biomaterial-based strategies, as it utilizes autologous or donor-derived mitochondria that possess inherent biocompatibility [72]. By integration with rationally designed biomaterials or therapies, transplanted mitochondria can be endowed with additional functionalities to support diverse therapeutic objectives, thus expanding the potential applications of this technology [71,73]. Notably, both preclinical studies and clinical trials have validated the effectiveness of mitochondrial therapies in treating various mitochondrial dysfunction-related diseases, such as acute lung injury [52], ischemic stroke [38], myocardial infarction [74], vascular diseases [33], pulmonary fibrosis [35,51], and single large-scale mitochondrial DNA deletion syndromes [75].

Herein we propose for the first time the development of mitochondrial therapies for IVDD, grounded on in-depth pathophysiological analysis of scRNA-seq data derived from human NP tissues. Mitochondria derived from rat cardiomyocytes can be effectively internalized by NPCs via endocytosis, resulting in their separate distribution and fusion with endogenous mitochondria in the cytoplasm. Moreover, the exogenous mitochondria internalized by NPCs would be transferred to neighboring cells through intercellular communication via TNTs. Leveraging these unique cellular distribution and transfer profiles, the transplanted mitochondria significantly enhanced ATP production, reduced mitochondrial membrane depolarization, and inhibited mitochondrial superoxide production in NPCs under pathological conditions. This was primarily achieved by improving mitochondrial biogenesis,

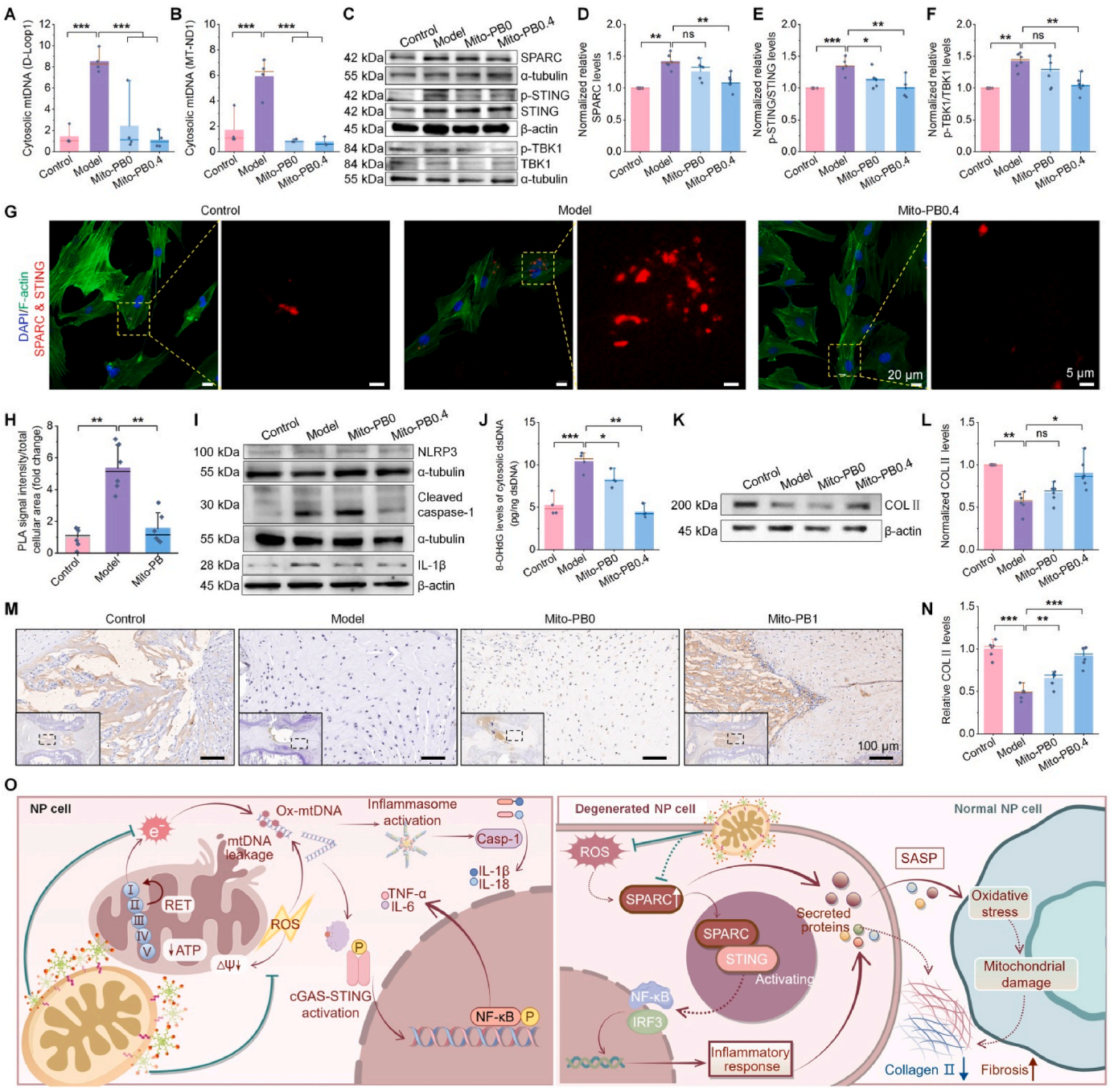

Fig. 9. Mito-PB alleviates IVDD by regulating mtDNA/SPARC-STING signaling. (A–B) qPCR quantification of cytosolic mtDNA levels using primers of either the non-coding D-Loop region (A, n = 4) or the coding MT-ND1 region (B, n = 3–4), which were normalized to mtDNA of total lysates from NPCs treated with different formulations. (C) Representative Western blot bands show protein levels of SPARC, STING, p-STING, TBK1, and p-TBK1 in NPCs subjected to various treatments. (D–F) Quantitative analysis of the levels of SPARC (D, n = 6), p-STING/STING (E, n = 5), and p-TBK1/TBK1 (F, n = 6). (G–H) Representative PLA images (G) and quantification (H) of the physical interaction intensities between SPARC and STING in NPCs (n = 6). Images in the right panels of (G) denote local magnification of red fluorescence signals for the regions indicated by the yellow-dashed rectangles. (I) Typical Western blot bands illustrate the relative protein levels of NLRP3, cleaved caspase-1, and IL-1β in NPCs post different treatments. (J) Quantified 8-OHdG levels of cytosolic dsDNA in NPCs (n = 4). (K–L) Western blot bands (K) and quantitative analysis (L) of COLLII levels in NPCs (n = 6). (M–N) Immunohistochemistry images (M) and quantitative analysis (N) of COLLII levels in the disc tissues from rats treated with different formulations (n = 6). The insets display low-magnification images. (O) A diagram illustrates that therapeutic effects of Mito-PB are associated with the regulation of the mtDNA-cGAS-STING axis and oxidized mtDNA (Ox-mtDNA)-NLRP3 axis (the left panel) as well as the SPARC-STING axis (the right panel) in NPCs during IVDD. Images in (O) were created with Figdraw.com. Data are presented as means ± SD. Statistical differences were determined using the one-way ANOVA with posthoc LSD or Tamhane's tests. *P < 0.05, **P < 0.01, and ***P < 0.001; ns, no significance.

promoting mitophagy, and regulating mitochondrial dynamics. Correspondingly, intradiscal transplantation of exogenous mitochondria effectively inhibited the progression of puncture-induced IVDD in rats, as evidenced in both short- and long-term studies, mainly by maintaining mitochondrial homeostasis and alleviating the structural abnormalities in the NP. Additionally, exogenous mitochondria were engineered with a bioactive, mitochondrial-targeting macromolecule to impart anti-oxidative and anti-inflammatory activities. The

functionalized multi-bioactive mitochondrial therapy demonstrated notably enhanced efficacy in alleviating IVDD in rats, mechanistically by regulating the mtDNA/SPARC-STING axis.

To the best of our knowledge, this study represents the first investigation of mitochondria-based therapies in an animal model of IVDD. However, several critical challenges must be addressed to facilitate clinical translation and advance this promising technique. First, the acquisition of high-quality, functional mitochondria is essential, yet the large-scale production and long-term storage of these organelles pose significant obstacles. Future research should focus on the optimization of mitochondrial isolation protocols and transplantation techniques to enhance post-transplantation survival rates and functional stability. Second, although our studies have not detected significant immune responses, comprehensive safety evaluations are still necessary. Previous findings indicate that transplantation of allogenic or xenogeneic mitochondria may carry genetic risks associated with mtDNA, potentially resulting in cumulative effects of mutations [76]. Consequently, mitochondrial transplantation procedures must incorporate rigorous screening and systematic evaluation processes to ensure genetic stability and safety. Furthermore, the therapeutic efficacy and safety profiles of these treatment regimens should be validated in large animal models to better predict clinical outcomes. Finally, the cost-effectiveness of mitochondrial transplantation necessitates thorough investigation through comprehensive studies to ensure the feasibility of clinical implementation.

Overall, the development of biomimetic therapeutic options, guided by scRNA-seq and characterized by rational functional integration, opens new avenues for the treatment of IVDD. Our findings underscore the therapeutic potential of engineered mitochondrial therapies in addressing this disorder. Moreover, the foundational design principles established in this study may be extrapolated to crate targeted therapies for other musculoskeletal diseases linked to mitochondrial dysfunction, such as osteoarthritis, rheumatoid arthritis, osteoporosis, and fibromyalgia.

CRediT authorship contribution statement

Guoyu Yang: Writing – review & editing, Writing – original draft, Methodology, Investigation, Formal analysis. **Chenpeng Dong:** Methodology, Investigation. **Zhaoxi Wu:** Investigation. **Peng Wu:** Investigation. **Cao Yang:** Supervision. **Lanlan Li:** Writing – original draft, Project administration, Investigation. **Jianxiang Zhang:** Writing – review & editing, Supervision, Project administration, Funding acquisition, Conceptualization. **Xinghuo Wu:** Supervision, Project administration, Funding acquisition.

Ethics approval and consent to participate

All animal experiments were conducted in accordance with the Guide for the Care and Use of Laboratory Animals proposed by National Institutes of Health. All experimental procedures and protocols were approved by the Animal Ethics Committee at Third Military Medical University (Army Medical University, Chongqing, China), approval No. AMUWEC20210946.

This work does not use human subjects.

Declaration of competing interest

The authors declare that they have no known competing financial interests or personal relationships that could have appeared to influence the work reported in this paper.

Acknowledgments

This work was supported by the National Natural Science Foundation of China (No. 81974349), Natural Science Foundation of Hubei Province (No. 2024AFD257), and the Graduate Supervisor Team Program of Chongqing in 2022.

Appendix A. Supplementary data

Supplementary data to this article can be found online at https://doi.org/10.1016/j.bioactmat.2025.02.036.

References

[1] M.V. Risbud, I.M. Shapiro, Role of cytokines in intervertebral disc degeneration: pain and disc content, Nat. Rev. Rheumatol. 10 (2014) 44–56.
[2] U. Zehra, et al., Mechanisms and clinical implications of intervertebral disc calcification, Nat. Rev. Rheumatol. 18 (2022) 352–362.
[3] H.W. Chen, et al., Emerging role and therapeutic implication of mtor signalling in intervertebral disc degeneration, Cell Prolif. 56 (2023) e13338.
[4] N. Fine, et al., Intervertebral disc degeneration and osteoarthritis: a common molecular disease spectrum, Nat. Rev. Rheumatol. 19 (2023) 136–152.
[5] D.C. Zhu, et al., Altered metabolism and inflammation driven by post-translational modifications in intervertebral disc degeneration, Research 7 (2024) 350.
[6] I.L. Mohd Isa, S.L. Teoh, N.H. Mohd Nor, S.A. Mokhtar, Discogenic low back pain: anatomy, pathophysiology and treatments of intervertebral disc degeneration, Int. J. Mol. Sci. 24 (2023) 208.
[7] V. Francisco, et al., A new immunometabolic perspective of intervertebral disc degeneration, Nat. Rev. Rheumatol. 18 (2022) 47–60.
[8] L. Frapin, et al., Lessons learned from intervertebral disc pathophysiology to guide rational design of sequential delivery systems for therapeutic biological factors, Adv. Drug Deliv. Rev. 149 (2019) 49–71.
[9] J. Clouet, M. Fusellier, A. Camus, C. Le Visage, J. Guicheux, Intervertebral disc regeneration: from cell therapy to the development of novel bioinspired endogenous repair strategies, Adv. Drug Deliv. Rev. 146 (2019) 306–324.
[10] A.L.A. Binch, J.C. Fitzgerald, E.A. Growney, F. Barry, Cell-based strategies for ivd repair: clinical progress and translational obstacles, Nat. Rev. Rheumatol. 17 (2021) 158–175.
[11] T.J. DiStefano, et al., Extracellular vesicles as an emerging treatment option for intervertebral disc degeneration: therapeutic potential, translational pathways, and regulatory considerations, Adv. Healthcare Mater. 11 (2022) e2100596.
[12] H.H. Genedy, et al., Microrna-targeting nanomedicines for the treatment of intervertebral disc degeneration, Adv. Drug Deliv. Rev. 207 (2024) 115214.
[13] W. Chen, et al., Circadian clock regulation via biomaterials for nucleus pulposus, Adv. Mater. 35 (2023) e2301037.
[14] Z. Li, et al., Oxygen metabolism-balanced engineered hydrogel microspheres promote the regeneration of the nucleus pulposus by inhibiting acid-sensitive complexes, Bioact. Mater. 24 (2023) 346–360.
[15] W. Liu, Z. Ma, Y. Wang, J. Yang, Multiple nano-drug delivery systems for intervertebral disc degeneration: current status and future perspectives, Bioact. Mater. 23 (2023) 274–299.
[16] F. Colella, et al., Drug delivery in intervertebral disc degeneration and osteoarthritis: selecting the optimal platform for the delivery of disease-modifying agents, J. Contr. Release 328 (2020) 985–999.
[17] A.P. Peredo, et al., Tension-activated nanofiber patches delivering an anti-inflammatory drug improve repair in a goat intervertebral disc herniation model, Sci. Transl. Med. 15 (2023) eadf1690.
[18] H. Wang, et al., Decoding the annulus fibrosus cell atlas by scrna-seq to develop an inducible composite hydrogel: a novel strategy for disc reconstruction, Bioact. Mater. 14 (2022) 350–363.
[19] J.X. Chen, et al., High-performance multi-dynamic bond cross-linked hydrogel with spatiotemporal sirna delivery for gene-cell combination therapy of intervertebral disc degeneration, Adv. Sci. 10 (2023) e2206306.
[20] L. Luo, et al., Injectable cartilage matrix hydrogel loaded with cartilage endplate stem cells engineered to release exosomes for non-invasive treatment of intervertebral disc degeneration, Bioact. Mater. 15 (2022) 29–43.
[21] D. Wu, et al., Repair strategies and bioactive functional materials for intervertebral disc, Adv. Funct. Mater. 32 (2022) 2209471.
[22] J. Bian, et al., Modulation of local overactive inflammation via injectable hydrogel microspheres, Nano Lett. 21 (2021) 2690–2698.
[23] A.R. Zhang, et al., Emerging tissue engineering strategies for annulus fibrosus therapy, Acta Biomater. 167 (2023) 1–15.
[24] Z.H. Chen, et al., Mechanical signal-tailored hydrogel microspheres recruit and train stem cells for precise differentiation, Adv. Mater. 35 (2023) e2300180.
[25] X. Tan, et al., Integrin and syndecan binding peptide-conjugated alginate hydrogel for modulation of nucleus pulposus cell phenotype, Biomaterials 277 (2021) 121113.
[26] K.W. Chung, et al., Mitochondrial damage and activation of the sting pathway lead to renal inflammation and fibrosis, Cell Metab. 30 (2019) 784–799.
[27] Z.W. Liao, et al., Metformin facilitates mesenchymal stem cell-derived extracellular nanovesicles release and optimizes therapeutic efficacy in intervertebral disc degeneration, Biomaterials 274 (2021) 120850.
[28] H. Zhou, et al., Role of oxidative stress in mitochondrial dysfunction and their implications in intervertebral disc degeneration: mechanisms and therapeutic strategies, J. Orthop. Translat. 49 (2024) 181–206.
[29] J. Tu, et al., Single-cell transcriptome profiling reveals multicellular ecosystem of nucleus pulposus during degeneration progression, Adv. Sci. 9 (2022) 2103631.

[30] Z. Sun, B. Liu, Z.J. Luo, The immune privilege of the intervertebral disc: implications for intervertebral disc degeneration treatment, Int. J. Med. Sci. 17 (2020) 685–692.
[31] M.J. Schafer, et al., Cellular senescence mediates fibrotic pulmonary disease, Nat. Commun. 8 (2017) 14532.
[32] T. Kitani, D. Kami, S. Matoba, S. Gojo, Internalization of isolated functional mitochondria: involvement of macropinocytosis, J. Cell Mol. Med. 18 (2014) 1694–1703.
[33] R.Z. Lin, et al., Mitochondrial transfer mediates endothelial cell engraftment through mitophagy, Nature 629 (2024) 660–668.
[34] A. Chi, et al., Stem leydig cells support macrophage immunological homeostasis through mitochondrial transfer in mice, Nat. Commun. 15 (2024) 2120.
[35] T. Huang, et al., Efficient intervention for pulmonary fibrosis via mitochondrial transfer promoted by mitochondrial biogenesis, Nat. Commun. 14 (2023) 5781.
[36] J.G. Baldwin, et al., Intercellular nanotube-mediated mitochondrial transfer enhances t cell metabolic fitness and antitumor efficacy, Cell 187 (2024) 6614–6630.
[37] K. Hayakawa, et al., Transfer of mitochondria from astrocytes to neurons after stroke, Nature 535 (2016) 551–555.
[38] J. Zhou, et al., Astrocytic lrp1 enables mitochondria transfer to neurons and mitigates brain ischemic stroke by suppressing arf1 lactylation, Cell Metab. 36 (2024) 2054–2068.
[39] R. Nakai, et al., Mitochondria transfer-based therapies reduce the morbidity and mortality of leigh syndrome, Nat. Metab. 6 (2024) 1886–1896.
[40] N. Borcherding, J.R. Brestoff, The power and potential of mitochondria transfer, Nature 623 (2023) 283–291.
[41] A. Rustom, R. Saffrich, I. Markovic, P. Walther, H.H. Gerdes, Nanotubular highways for intercellular organelle transport, Science 303 (2004) 1007–1010.
[42] D. Liu, et al., Intercellular mitochondrial transfer as a means of tissue revitalization, Signal Transduct. Targeted Ther. 6 (2021) 65.
[43] T. Wai, T. Langer, Mitochondrial dynamics and metabolic regulation, Trends Endocrinol. Metabol. 27 (2016) 105–117.
[44] P. Mitchell, Coupling of phosphorylation to electron and hydrogen transfer by a chemi-osmotic type of mechanism, Nature 191 (1961) 144–148.
[45] F. Scialò, D.J. Fernández-Ayala, A. Sanz, Role of mitochondrial reverse electron transport in ros signaling: potential roles in health and disease, Front. Physiol. 8 (2017) 428.
[46] J.N.S. Vargas, M. Hamasaki, T. Kawabata, R.J. Youle, T. Yoshimori, The mechanisms and roles of selective autophagy in mammals, Nat. Rev. Mol. Cell Biol. 24 (2023) 167–185.
[47] R.J. Youle, A.M. van der Bliek, Mitochondrial fission, fusion, and stress, Science 337 (2012) 1062–1065.
[48] E.E. Griffin, S.A. Detmer, D.C. Chan, Molecular mechanism of mitochondrial membrane fusion, Biochim. Biophys. Acta 1763 (2006) 482–489.
[49] J.W. Larson 3rd, E.A. Levicoff, L.G. Gilbertson, J.D. Kang, Biologic modification of animal models of intervertebral disc degeneration, J. Bone Joint Surg. 88 (2006) 83–87.
[50] J. Dowdell, et al., Intervertebral disk degeneration and repair, Neurosurgery 80 (2017) S46–s54.
[51] T. Huang, et al., Iron oxide nanoparticles augment the intercellular mitochondrial transfer–mediated therapy, Sci. Adv. 7 (2021) eabj0534.
[52] M.N. Islam, et al., Mitochondrial transfer from bone-marrow-derived stromal cells to pulmonary alveoli protects against acute lung injury, Nat. Med. 18 (2012) 759–765.
[53] S. Liu, et al., An osteoimmunomodulatory biopatch potentiates stem cell therapies for bone regeneration by simultaneously regulating il-17/ferroptosis signaling pathways, Adv. Sci. (2024) e2401882.
[54] E.L. Mills, et al., Succinate dehydrogenase supports metabolic repurposing of mitochondria to drive inflammatory macrophages, Cell 167 (2016) 457–470.
[55] L. Peruzzotti-Jametti, et al., Mitochondrial complex i activity in microglia sustains neuroinflammation, Nature 628 (2024) 195–203.
[56] D. Sakai, et al., Exhaustion of nucleus pulposus progenitor cells with ageing and degeneration of the intervertebral disc, Nat. Commun. 3 (2012) 1264.
[57] S. Ryu, et al., The matricellular protein sparc induces inflammatory interferon-response in macrophages during aging, Immunity 55 (2022) 1609–1626.e1607.
[58] L.S. Huang, et al., Mtdna activates cgas signaling and suppresses the yap-mediated endothelial cell proliferation program to promote inflammatory injury, Immunity 52 (2020) 475–486.e475.
[59] M.F. Gulen, et al., Cgas–sting drives ageing-related inflammation and neurodegeneration, Nature 620 (2023) 374–380.
[60] N.V. Vo, et al., Expression and regulation of metalloproteinases and their inhibitors in intervertebral disc aging and degeneration, Spine J. 13 (2013) 331–341.
[61] J.D. McCully, S. Levitsky, P.J. Del Nido, D.B. Cowan, Mitochondrial transplantation for therapeutic use, Clin. Transl. Med. 5 (2016) 16.
[62] J.L. Larson-Casey, C. He, A.B. Carter, Mitochondrial quality control in pulmonary fibrosis, Redox Biol. 33 (2020) 101426.
[63] F.J. Lyu, et al., Ivd progenitor cells: a new horizon for understanding disc homeostasis and repair, Nat. Rev. Rheumatol. 15 (2019) 102–112.
[64] K. Sun, X. Jing, J. Guo, X. Yao, F. Guo, Mitophagy in degenerative joint diseases, Autophagy 17 (2021) 2082–2092.
[65] Y. Song, et al., Sirtuin 3-dependent mitochondrial redox homeostasis protects against ages-induced intervertebral disc degeneration, Redox Biol. 19 (2018) 339–353.
[66] L. Kang, et al., Restoration of autophagic flux rescues oxidative damage and mitochondrial dysfunction to protect against intervertebral disc degeneration, Oxid. Med. Cell. Longev. 2019 (2019) 7810320.
[67] C. Liu, et al., A redox homeostasis modulatory hydrogel with glrx3+ extracellular vesicles attenuates disc degeneration by suppressing nucleus pulposus cell senescence, ACS Nano 17 (2023) 13441–13460.
[68] Y. Wang, et al., Repair of degenerative nucleus pulposus by polyphenol nanosphere-encapsulated hydrogel gene delivery system, Biomaterials 298 (2023) 122132.
[69] H. Zhou, et al., Microenvironment-responsive metal-phenolic network release platform with ros scavenging, anti-pyroptosis, and ecm regeneration for intervertebral disc degeneration, Bioact. Mater. 37 (2024) 51–71.
[70] Q. Chen, et al., Mitochondrial-targeted metal-phenolic nanoparticles to attenuate intervertebral disc degeneration: alleviating oxidative stress and mitochondrial dysfunction, ACS Nano 18 (2024) 8885–8905.
[71] J. Xu, et al., Targeted transplantation of engineered mitochondrial compound promotes functional recovery after spinal cord injury by enhancing macrophage phagocytosis, Bioact. Mater. 32 (2024) 427–444.
[72] A. Masuzawa, et al., Transplantation of autologously derived mitochondria protects the heart from ischemia-reperfusion injury, Am. J. Physiol. Heart Circ. Physiol. 304 (2013) H966–H982.
[73] X. Sun, et al., Intravenous transplantation of an ischemic-specific peptide-tpp-mitochondrial compound alleviates myocardial ischemic reperfusion injury, ACS Nano 17 (2023) 896–909.
[74] B. Shin, et al., A novel biological strategy for myocardial protection by intracoronary delivery of mitochondria: safety and efficacy, JACC Basic Transl. Sci. 4 (2019) 871–888.
[75] E. Jacoby, et al., Mitochondrial augmentation of hematopoietic stem cells in children with single large-scale mitochondrial DNA deletion syndromes, Sci. Transl. Med. 14 (2022) eabo3724.
[76] D.P. Wolf, T. Hayama, S. Mitalipov, Mitochondrial genome inheritance and replacement in the human germline, EMBO J. 36 (2017) 2177–2181.